J. Fluid Mech. (2012), *vol.* 712, *pp.* 244–272.
doi:10.1017/jfm.2012.417

Triggering turbulence efficiently in plane Couette flow

S. M. E. Rabin[1]†, C. P. Caulfield[2,1] and R. R. Kerswell[3]

[1] Department of Applied Mathematics & Theoretical Physics, Centre for Mathematical Sciences, University of Cambridge, Wilberforce Road, Cambridge CB3 0WA, UK

[2] BP Institute, University of Cambridge, Madingley Rise, Madingley Road, Cambridge CB3 0EZ, UK

[3] School of Mathematics, University of Bristol, Bristol BS8 1TW, UK

(Received 29 November 2011; revised 18 June 2012; accepted 16 August 2012; first published online 27 September 2012)

We use a variational formulation incorporating the full Navier–Stokes equations to identify initial perturbations with finite kinetic energy E_0 which generate the largest gain in perturbation kinetic energy at some time T later for plane Couette flow. Using the flow geometry originally used by Butler & Farrell (*Phys. Fluids* A, vol. 4, 1992, pp. 1637–1650) to identify the linear transient optimal perturbations for $E_0 \to 0$ and incorporating T as part of the optimization procedure, we show how the addition of nonlinearity smoothly changes the result as E_0 increases from zero until a small but finite E_c is reached. At this point, the variational algorithm is able to identify an initial condition of completely different form which triggers turbulence – called the *minimal seed* for turbulence. If instead T is fixed at some asymptotically large value, as suggested by Pringle, Willis & Kerswell (*J. Fluid Mech.*, vol. 703, 2012, pp. 415–443), a fundamentally different 'final' optimal perturbation emerges from our algorithm above some threshold initial energy $E_f \in (0, E_c)$ which shows signs of localization. This nonlinear optimal perturbation clearly approaches the structure of the minimal seed as $E_0 \to E_c^-$, although for $E_0 < E_c$, its maximum gain over all time intervals is always less than the equivalent maximum gain for the 'quasi-linear optimal perturbation', i.e. the finite-amplitude manifestation of the underlying linear optimal perturbation. We also consider a wider flow geometry recently studied by Monokrousos *et al.* (*Phys. Rev. Lett.*, vol. 106, 2011, 134502) and present evidence that the critical energy for transition E_c they found by using total dissipation over a time interval as the optimizing functional is recovered using energy gain at a fixed target time as the optimizing functional, with the same associated minimal seed emerging. This emphasizes that the precise form of the functional does not appear to be important for identifying E_c provided it takes heightened values for turbulent flows, as postulated by Pringle, Willis & Kerswell (*J. Fluid Mech.*, vol. 703, 2012, pp. 415–443). All our results highlight the irrelevance of the linear energy gain optimal perturbation for predicting or describing the lowest-energy flow structure which triggers turbulence.

Key words: nonlinear instability, transition to turbulence, variational methods

† Email address for correspondence: S.Rabin@damtp.cam.ac.uk

1. Introduction

The investigation of hydrodynamic stability is one of the canonical problems of fluid dynamics. A particularly interesting archetypal flow is plane Couette flow (PCF), i.e. the flow between two parallel plates separated by a distance $2h$ moving at a relative velocity $2U$. PCF is linearly stable for all $Re = Ud/\nu$ (Romanov 1973), where ν is the fluid's kinematic viscosity, yet turbulence has been observed experimentally as low as $Re = 325$ (Bottin & Chate 1998). It has been hypothesized that transient perturbation growth, due to the non-normality of the underlying linear operator of the Navier–Stokes equations, may explain this disconnect. Several authors (e.g. Gustavsson 1991, Butler & Farrell 1992, Reddy & Henningson 1993) demonstrated that substantial transient kinetic energy gain $G(T) = E(T)/E(0)$ (where $E(T)$ is the infinitesimally small kinetic energy at the final 'target' time T of the chosen optimization interval) could be achieved by a linear (infinitesimal) optimal perturbation (see Schmid 2007 for a review). Henceforth, we shall refer to such a perturbation as a LOP_T (see glossary), where the subscript T denotes the particular specific target time T chosen. The optimal gain for such perturbations can be quite large, with maximum values for $Re \simeq 1000$ of $G \simeq O(1000)$ for $T = T_L = O(100)$, where T_L is the time at which the transient perturbation reaches its maximum energy amplitude, as shown by Butler & Farrell (1992). Proponents of such an essentially linear mechanism for energy growth point to the Reynolds–Orr equation (Schmid 2007) as an indication that energy growth is a linear effect because $\mathrm{d}E/\mathrm{d}t$ is independent of the nonlinear advective terms in the Navier–Stokes equations. The argument is that if a real flow is seeded with a 'small' yet finite amplitude perturbation with the same structure as a LOP_T, the transient energy gain formally identified for the LOP_T when its amplitude is assumed infinitesimal could be sufficiently large to 'push' the perturbation into a finite-amplitude nonlinear regime where the perturbation affects the base flow, and hence perhaps to trigger transition.

However, this line of thinking is based on a couple of implicit assumptions: that the entrance into the nonlinear regime of this specific class of perturbation, determined through consideration of a formally linear problem, will lead to turbulence; and that the so-determined linear optimal perturbation (LOP_T) is still the 'best' choice for the growth of inherently nonlinear, finite-amplitude perturbations. Furthermore, it is not *a priori* clear what the most appropriate choice for the optimization time T is, though an obvious choice might be the time T_L which maximizes the gain across all possible time intervals within the linear problem.

Perhaps the more significant assumption that the LOP_T is the 'best' choice even for nonlinear problems can be explicitly probed by posing the optimal growth problem for initial perturbations of finite amplitude which can affect the base flow as they grow. This has been done recently for pipe flow (Pringle & Kerswell 2010, henceforth referred to as PK10) and boundary layer flow (Cherubini *et al.* 2010, 2011*a*,*b*); see also Duguet, Brandt & Larsson (2010) for preliminary work in plane Couette flow. Within such studies, as the initial energy of the perturbation increases from arbitrarily small values, it is natural to find a finite-amplitude perturbation which can be directly related to the formally linear optimal perturbations discussed above. In this paper, we shall refer to such a finite amplitude perturbation as a 'quasi-linear optimal perturbation' or 'QLOP_T' to make explicit its connection with the previously considered linear problem, with the subscript T, as before, denoting the optimization time interval for the particular optimization problem considered. All these recent studies did identify such perturbations, whose maximal energy gain (over all time

intervals) typically does occur for an optimization time interval T_Q quite close to T_L, the 'best' time interval for the linear problem.

Interestingly, they also discovered the existence of inherently nonlinear optimal perturbations which have a very different structure to the quasi-linear optimal perturbations. We shall refer to such a qualitatively different optimal perturbation as an 'NLOP$_T$', where as before T denotes the optimization time interval. For the same flow geometry, parameters and optimization time interval T, the NLOP$_T$, which PK10 and Cherubini *et al.* (2010) identified, has a larger gain than the QLOP$_T$ beyond a small but finite energy threshold, and so naturally emerged as the dominant optimal perturbation. Unfortunately, PK10 were unable to investigate whether the NLOP$_T$ played any role in triggering transition, or to determine the critical initial perturbation energy threshold 'E_c' to lead to a turbulent state, because of convergence issues. However, a follow-up study, Pringle, Willis & Kerswell (2012) (henceforth referred to as PWK12), with a more efficient code run at higher resolution succeeded in identifying the NLOP$_T$ for larger initial energies. At $E_0 = E_{fail}$, they again found a failure to converge but noticed that this corresponded to their optimization algorithm encountering turbulent (end) flows. The conclusion was that this failure energy E_{fail} is sufficiently large to enable an initial perturbation to undergo the transition to turbulence: i.e. $E_{fail} \geqslant E_c$. In dynamical systems parlance, this initial perturbation is then in the basin of attraction of the turbulence, or more generally (if the turbulence is actually not an attractor but a chaotic saddle), has crossed the 'edge', a hypersurface which separates initial conditions which become turbulent from those which relaminarize (Itano & Toh 2001; Skufca, Yorke & Eckhardt 2006; Schneider, Eckhardt & Yorke 2007; Duguet, Willis & Kerswell 2008). The picture then put forward by PWK12 is that as E_0 increases from 0, the $E = E_0$ hypersurface in phase space intersects the edge for the first time at $E_0 = E_c$ and that the initial perturbation which corresponds to their (generically unique) intersection at $E_0 = E_c$ is the 'minimal seed' for triggering turbulence. This seed is 'minimal' in the sense that it is the lowest-energy state on the edge and therefore represents the most energy-efficient way of triggering turbulence by adding an infinitesimal perturbation to it. PWK12 also find evidence to suggest that there is an identifiable (and hence unique) NLOP$_T$ (in the nomenclature we are using here, qualitatively different from the QLOP$_T$) which tends to the minimal seed associated with this loss of convergence (and transition to turbulence) as $E_0 \to E_c^-$. PWK12 summarize their thinking as two conjectures.

> **Conjecture 1.** *For T sufficiently large, the initial energy value E_{fail} at which the energy growth problem first fails (as E_0 is increased) to have a smooth optimal solution will correspond exactly to E_c.*
>
> **Conjecture 2.** *For T sufficiently large, the optimal initial condition for maximal energy growth at $E_0 = E_c - \epsilon^2$ converges to the minimal seed at E_c as $\epsilon \to 0$.*

It is important to stress that these conjectures actually do not take a position on the relevance of the results of the linear optimization problem to the transition to turbulence. In principle, it is possible that the 'optimal initial condition for maximal energy growth at $E_0 = E_c - \epsilon^2$' corresponds to QLOP$_T$. The evidence from both PWK12 and Cherubini *et al.* (2010, 2011*a*,*b*), however, suggests that another distinct state, NLOP$_T$, emerges for sufficiently large E_0, and PWK12 observe that this particular 'final' NLOP$_T$ connects smoothly with the minimal seed as $E_0 \to E_c^-$ (Cherubini *et al.* use a relatively small T and actually achieve convergence for $E_0 > E_c$ because of this.) We will henceforth refer to this 'final' optimal as NLOP$_T^{(f)}$ which, like QLOP$_T$, can be thought of as a solution branch of the optimization procedure

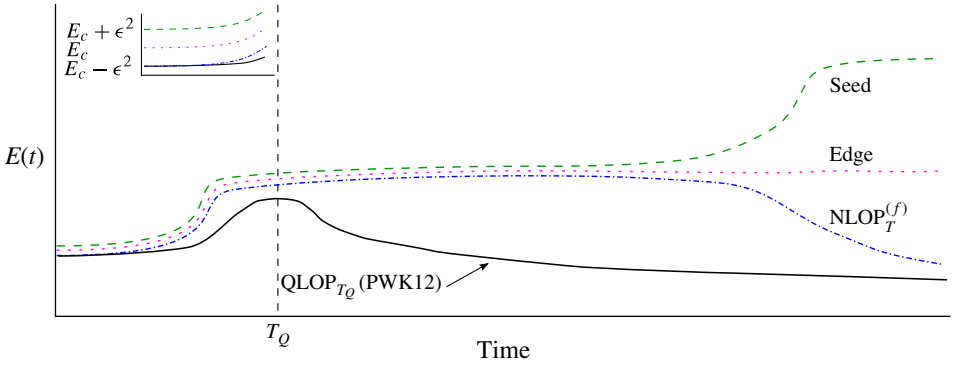

FIGURE 1. (Colour online) Schematic representation of the time evolution of the energy of perturbations in pipe flow with initial energies close to E_c found in PWK12. The final nonlinear optimal perturbation $\text{NLOP}_T^{(f)}$ with initial energy $E_c - \epsilon^2$, and which approaches the minimal seed as $\epsilon \to 0$, is plotted with a dot-dashed blue line, the edge state which connects to the minimal seed with initial energy E_c is plotted with a dotted magenta line, and a turbulent seed with initial energy $E_c + \epsilon^2$ is plotted with a dashed green line. The $\text{NLOP}_T^{(f)}$ and the turbulent seed both approach a plateau of substantial and approximately constant energy gain for a significant period of time, sandwiching (as shown in the blown-up inset) the time evolution of the edge state for which the minimal seed is the lowest-energy state and initial condition. This plateau is larger than the maximum gain of the QLOP_{T_Q} at T_Q (plotted with a thin black line).

parametrized by the initial energy E_0. Indeed, for sufficiently large initial energies, the evidence presented by PWK12 suggests that this distinct $\text{NLOP}_T^{(f)}$ solution branch always has a larger gain than the associated QLOP_T, even over short time intervals $T < T_Q \simeq T_L$. This is illustrated schematically in figure 1, which shows the time-dependent behaviour of the different solution branches when E_0 is close to E_c. The evolution of the perturbation with initial energy $E_c - \epsilon^2$, which maximizes energy gain over the fixed time interval T, and which we refer to as an $\text{NLOP}_T^{(f)}$, is shown with a dot-dashed blue line. This perturbation grows towards a finite-amplitude plateau of energy for a substantial period of time, before ultimately decaying and relaminarizing. The plateau reflects the simplest, steady case of an 'edge state' (attracting state for edge-confined dynamics) and is plotted with a dotted magenta line. The minimal energy for this edge state is E_c, which occurs at time $t = 0$ for the 'minimal seed' flow structure, by definition. We also plot (with a dashed green line) the time evolution of a turbulent seed with initial energy $E_c + \epsilon^2$, which ultimately reaches an even higher, turbulent energy state, having first spent a non-trivial period of time with energy close to this intermediate energy plateau. Finally, we plot the time evolution of the QLOP_{T_Q} (plotted with a thin black solid line, and labelled as the QLOP_{T_Q} (PWK12)) with initial energy $E_c - \epsilon^2$. We believe the qualitative behaviour of this QLOP_T is generic for sufficiently large target times, in the sense that the particular initial structure of the quasi-linear optimal perturbation and its time evolution does not depend strongly on the specific target time T chosen, although the associated gain does change markedly. At this initial energy, although the QLOP_T still grows to have a substantial peak gain at a time $T_Q \simeq T_L$ (marked with a vertical line), this gain is always below that of the $\text{NLOP}_T^{(f)}$ for all times, and so, at least for initial energies this close to the critical energy E_c, the QLOP_T plays no role in the optimization problem.

In this paper, we wish to investigate further the generic validity of the conjectures of PWK12 in the context of PCF, paying particular attention to whether the QLOP_T has any relevance to the minimal seed. We consider two sets of geometry and Reynolds numbers for PCF. Principally, we consider the geometry discussed by Butler & Farrell (1992) (henceforth referred to as BF92): a relatively narrow spanwise domain with $Re = 1000$. BF92 investigated in detail the properties of the optimal perturbation which maximized the energy gain within a linearized problem for this geometry, and so it seems natural to consider a fully nonlinear optimization problem within the same geometry. The second geometry we consider has a double the spanwise domain width of BF92 with $Re = 1500$, considered recently in an inherently nonlinear study by Monokrousos *et al.* (2011) (henceforth referred to as M11). They identified a turbulent seed in PCF by considering a different variational problem to that of maximization of energy gain over a fixed time interval. They searched for a finite-amplitude initial condition which maximized the total energy dissipation over a long but fixed time interval (or equivalently the time-averaged dissipation rate). They purposely looked for a turbulent end state at the end of their optimization time interval, and then worked downwards in initial energy to identify the threshold for transition.

Most of our study is based around the BF92 geometry, but we believe it is useful to consider the M11 geometry for two particular reasons. Firstly, by considering two different flow geometries, we are able to investigate whether there is anything generic that can be said about the progression, as E_0 increases, of the optimal perturbations for 'long' time intervals starting with the (infinitesimal) linear optimal perturbation at $E_0 = 0$, and ultimately leading (possibly) to the final $\mathrm{NLOP}_T^{(f)}$ which then connects to the minimal seed at $E_0 = E_c$, i.e. if the second conjecture of PWK12 is true. Secondly, we can also compare our results (based around maximizing energy gain at a specific time horizon) to the results reported in M11 where the optimized functional was the total energy dissipation over the entire optimizing interval, to get some insight into whether the predicted minimal seed depends strongly on the particular form of the optimization problem being solved. Of principal interest will be whether this approach can identify E_c and the form of the minimal seed either directly (by smooth evolution of an explicitly identified $\mathrm{NLOP}_T^{(f)}$ as $E_0 \to E_c^-$) or indirectly (by failing to converge), which will address the conjecture that the energy E_{fail} at which the problem ceases to converge corresponds to E_c, the critical energy for the existence of a minimal seed.

Importantly for our investigation, the calculations reported here for PCF do not, however, show the same behaviour of the QLOP_T solution branch as indicated in figure 1. Specifically, in PCF, it appears that the energy plateau, attained at some sufficiently large target time T by the minimal seed with initial critical energy E_c, is not larger than the energy attained at earlier times by other nonlinear perturbations with initial energy E_c, although these other perturbations do subsequently decay and allow the flow to relaminarize. We sketch schematically in figure 2 two such scenarios, which as we show in this paper actually correspond to the time-dependent behaviour of PCF in the BF92 flow geometry and the M11 flow geometry respectively.

The principal difference between the pipe flow behaviour observed by PWK12 and that which appears to occur in PCF is the relative magnitude of the maximum energy attained by the QLOP_{T_Q} with initial energy close to E_c at time T_Q compared to the energy plateau attained by the minimal seed at longer times. As shown in figure 2(*a*), this maximum energy attained by the PCF QLOP_{T_Q} (plotted with a thick black line) is now larger than the energy plateau attained by the edge state (plotted with a magenta

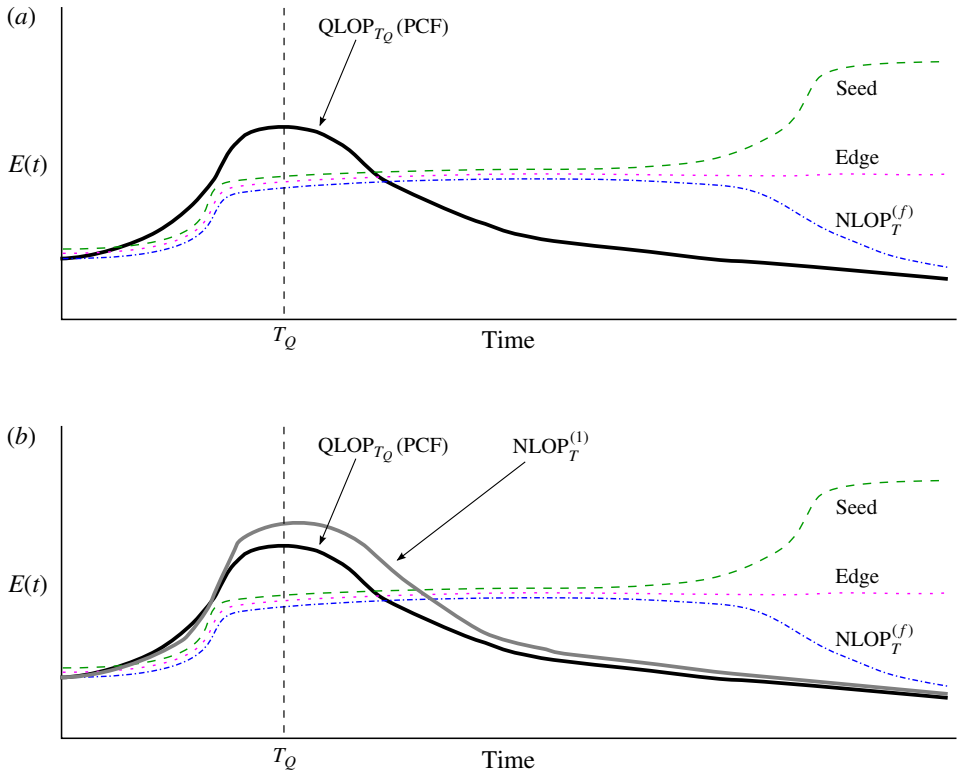

FIGURE 2. (Colour online) Schematic representations of two different scenarios for the time evolution of the energy of perturbations in PCF with initial energies close to E_c. The final nonlinear optimal perturbation NLOP$_T^{(f)}$ with initial energy $E_c - \epsilon^2$, and which approaches the minimal seed as $\epsilon \to 0$, is plotted with a dot-dashed blue line, the edge state which connects to the minimal seed with initial energy E_c is plotted with a dotted magenta line, and a turbulent seed with initial energy $E_c + \epsilon^2$ is plotted with a dashed green line. The NLOP$_T^{(f)}$ and the turbulent seed both approach a plateau of substantial and approximately constant energy gain for a significant period of time, sandwiching the time evolution of the edge state for which the minimal seed is the lowest energy state and initial condition. (*a*) The energy plateau of the edge state is significantly smaller than the peak energy gain for the relevant QLOP$_{T_Q}$ at T_Q (plotted with a thick black line), in the BF92 flow geometry and so the QLOP$_{T_Q}$ will dominate and 'mask' the NLOP$_T^{(f)}$ when optimizing over all time intervals until the edge is crossed. (*b*) In the M11 flow geometry in PCF there is now a new solution branch of nonlinear optimal perturbations labelled NLOP$_T^{(1)}$ and plotted with a thick grey line. This branch is distinct from and has larger gain than the QLOP$_{T_Q}$ (plotted with a thick black line), but still 'masks' the NLOP$_T^{(f)}$ when optimizing over all time intervals.

dotted line) and the final NLOP$_T^{(f)}$ (plotted with a blue dot-dashed line) conjectured to approach the minimal seed as $E_0 \to E_c^-$.

As specifically required by the conjectures of PWK12, over a sufficiently long time horizon, the QLOP$_T$ solution branch inevitably decays, and so the NLOP$_T^{(f)}$ will indeed be the optimal perturbation for maximizing energy gain for initial energies sufficiently close to E_c and sufficiently long optimization intervals T. Therefore, demonstrating that E_{fail}, where the optimization algorithm first fails to converge, corresponds to

E_c (the initial energy from which a minimal seed can lead to turbulence) is thus equivalent to establishing that the variational algorithm employed can indeed converge to the final $\mathrm{NLOP}_T^{(f)}$ solution branch for sufficiently long optimization time intervals. However, right up until E_c, it is entirely possible that the QLOP_{T_Q} will have larger peak energy gain than the $\mathrm{NLOP}_T^{(f)}$ for a given choice of T. Therefore, the emergence of the $\mathrm{NLOP}_T^{(f)}$ solution branch may be 'masked' by the quasi-linear optimal perturbation, unless sufficiently long optimization intervals, and initial energies sufficiently close to E_c, are chosen to ensure the decay of the QLOP_T and the existence of the $\mathrm{NLOP}_T^{(f)}$ solution branch. Such long time evolutions for initial energies close to the 'edge' are likely to be computationally demanding, as the solution state space may be quite non-smooth due to the incipient onset of the possibility of 'turbulent' flow. We discuss the computational challenge of this issue in more detail below.

Of course, such 'masking' could also occur due to the emergence of one or more other nonlinear optimal perturbation solution branches qualitatively different from the linear optimal perturbation. At intermediate finite initial energy amplitudes, such other nonlinear optimal perturbation solution branches could conceivably have globally (across all time horizons) larger energy gains than the QLOP_T solution branch and yet, right up to E_c, have larger energy gain than the final $\mathrm{NLOP}_T^{(f)}$ solution branch associated with the minimal seed. In figure 2(*b*), we show schematically just such a scenario, which, as we discuss below, actually occurs for PCF in the M11 geometry. The principal difference is that above a 'cross-over' initial energy E_1, i.e. for a range of initial energies $E_1 < E_0 < E_c$, a new qualitatively distinct nonlinear optimal perturbation appears (which we refer to as an $\mathrm{NLOP}_T^{(1)}$, plotted with a thick grey line). This solution branch attains a higher energy than the equivalent QLOP_T and the plateau associated with the edge state. In general, it is of course conceivable that there could well be a sequence of such solution branches, each having a window of initial energy perturbation for which the solution branch has the largest possible (across all optimization time intervals) energy gain. This scenario will also of course lead to 'masking' of the 'final' $\mathrm{NLOP}_T^{(f)}$ solution branch for all $E_0 < E_c$. In general the $\mathrm{NLOP}_T^{(f)}$ solution branch can be 'unmasked' by fixing T at a sufficiently large value as $E_0 \to E_c^-$. (In the scenario considered by PWK12, and shown schematically in figure 1, this 'masking' phenomenon does not arise, and the 'final' $\mathrm{NLOP}_T^{(f)}$ solution branch may be thought of as an $\mathrm{NLOP}_T^{(1)}$ solution branch, as it does experience a greater gain than the QLOP_{T_Q} for initial energies above some cross-over value E_1.)

To find turbulent seeds, we find it more efficient to develop further the conventional variational formulation to include optimization over T, the time horizon of the optimization time interval window or 'target time'. This means we are then able to identify the initial perturbation which achieves the highest gain possible over all T with the corresponding optimal time interval T_{opt} now an interesting output. Letting T_{opt} be an output of the optimization requires only a small adjustment in the algorithm, yet it has far-reaching consequences for the results, particularly in the context of PCF, due principally to the complicating properties of the transient energy gain of the relevant quasi-linear optimal perturbation, and the appearance of a new nonlinear optimal perturbation solution branch for intermediate energies $E_1 < E_0 < E_c$. In particular, if different solution branches 'mask' the emergence of the $\mathrm{NLOP}_T^{(f)}$ solution branch until the critical threshold $E_0 = E_c$ is reached and turbulent seeds can be identified with markedly higher energy gains, there will be a discontinuity in the

identified globally optimal time interval T_{opt}, with T_{opt} jumping to substantially larger values once the initial energy amplitude E_0 crosses E_c and so the turbulent seeds become accessible.

To describe the results of our investigation into the validity of the conjectures of PWK12, and also the properties of the identified optimal perturbations as initial energy, optimization time interval, and PCF geometry are changed, the plan of the paper is as follows. In § 2 we briefly present the variational framework and discuss how the new target time optimization is carried out. In § 3 we discuss the results obtained for the BF92 flow geometry. We describe the structure and properties of the QLOP_T solution branch for finite initial energies E_0, demonstrate that the algorithm converges adequately, and also identify the specific time interval T_Q where the energy gain for the QLOP_T is maximized across all possible time intervals. We identify the critical energy for turbulence E_c, showing that the 'masking' phenomenon shown in figure 2 does indeed appear to occur. We discuss the structure and time evolution of the associated minimal seed, and show that a perturbation of this form does evolve towards an elevated plateau in energy for a non-trivial period of time, and then diverges from this (apparent) near-approach to the edge state towards turbulence, consistent with the schematic picture shown in figure 2. By rescaling the amplitude of this minimal seed down below E_c and considering a range of fixed optimization intervals, we gather convincing evidence for the existence of an $\mathrm{NLOP}_T^{(f)}$ converging to the minimal seed, and hence support for the two key conjectures of PWK12. In § 4 we then discuss our results for the M11 flow geometry, paying particular attention to comparing our results for this flow geometry both to our BF92 results and the previously reported results of M11. For intermediate initial energies, the greater spanwise extent and higher Re of this flow geometry appears to allow the dominance of a spatially localized nonlinear optimal perturbation inherently different from the QLOP_T, i.e. an $\mathrm{NLOP}_T^{(1)}$ as shown schematically in figure 2(*b*). The time evolution of this $\mathrm{NLOP}_T^{(1)}$ appears to lead towards behaviour very reminiscent of the QLOP_T after an initial period of 'unpacking', which allows for somewhat enhanced perturbation energy gain compared to the equivalent QLOP_T. Interestingly, we find that the critical value of energy E_c for the identification of the minimal seed for our energy gain optimization problem is entirely consistent with that identified by M11 for their total dissipation optimization problem. Armed with these results, we draw our conclusions in § 5, speculating further on the extent to which we believe our results and the above-quoted conjectures of PWK12 are generically applicable.

2. Variational framework

In essence, we seek the initial disturbance (at time $t = 0$) of kinetic energy E_0 to a laminar flow which attains the largest relative energy growth or 'gain' $G(T) := E(T)/E_0$ a time T later while evolving under the Navier–Stokes equations, remaining incompressible and respecting the applied boundary conditions. Here $E(T) := \langle \boldsymbol{u}(T), \boldsymbol{u}(T) \rangle / 2$, with the angle brackets implying the integral inner product

$$\langle \boldsymbol{v}, \boldsymbol{u} \rangle := \frac{1}{V} \int_{\mathscr{D}} \boldsymbol{v}^\dagger \boldsymbol{u} \, \mathrm{d}V, \tag{2.1}$$

where † denotes the Hermitian conjugate, and V is the volume of the domain $\mathscr{D}$. We consider plane Couette flow (PCF) using a coordinate system such that the streamwise direction is x, the wall normal direction is y and the spanwise direction is z. The x and z directions are assumed to be periodic and the separation between the walls ($2h$) is

used to scale lengths so that the positions of the walls are given by $y = \pm 1$. The speed difference between the walls ($2U$) scales the velocity so that the non-dimensionalized background Couette flow is $\boldsymbol{U}(y) = y\boldsymbol{e}_x$ and the Reynolds number $Re := Uh/\nu$.

As noted in § 1, the functional which we choose to extremize is the energy gain which, when constrained by the Navier–Stokes equations, the initial energy value $E(0) = E_0$ and incompressibility, leads to the Lagrangian

$$\mathscr{L} := \frac{E(T)}{E_0} - [\partial_t \boldsymbol{u} + N(\boldsymbol{u}) + \boldsymbol{\nabla} p, \boldsymbol{v}] - [\boldsymbol{\nabla} \cdot \boldsymbol{u}, q] - \left(\frac{1}{2}\langle \boldsymbol{u}_0, \boldsymbol{u}_0\rangle - E_0\right) c - \langle \boldsymbol{u}(0) - \boldsymbol{u}_0, \boldsymbol{v}_0\rangle. \tag{2.2a}$$

In this equation, N is the nonlinear operator

$$N(u_i) := U_j \partial_j u_i + u_j \partial_j U_i + u_j \partial_j u_i - \frac{1}{Re}\partial_j \partial_j u_i, \tag{2.2b}$$

and square brackets denote a time average of the inner product,

$$[\boldsymbol{v}, \boldsymbol{u}] := \frac{1}{T}\int_0^T \langle \boldsymbol{v}, \boldsymbol{u}\rangle \, \mathrm{d}t. \tag{2.3}$$

In the Lagrangian, $\boldsymbol{v}$, q, $\boldsymbol{v}_0$ and c are Lagrange multipliers, $\boldsymbol{u}_0$ is the initial value of the perturbation velocity $\boldsymbol{u}$ and $\boldsymbol{U}$ the background Couette flow.

Taking first variations of the Lagrangian with respect to $\boldsymbol{v}$, q, $\boldsymbol{v}_0$ and c and setting them to zero recovers (respectively) the constraints of the Navier–Stokes equations, incompressibility, the initial kinetic energy of E_0 and initial state $\boldsymbol{u}_0 = \boldsymbol{u}(0)$,

$$\frac{\delta \mathscr{L}}{\delta \boldsymbol{v}} = \partial_t \boldsymbol{u} + N(\boldsymbol{u}) + \boldsymbol{\nabla} p := 0, \tag{2.4}$$

$$\frac{\delta \mathscr{L}}{\delta q} = \boldsymbol{\nabla} \cdot \boldsymbol{u} := 0, \tag{2.5}$$

$$\frac{\delta \mathscr{L}}{\delta \boldsymbol{v}_0} = \boldsymbol{u}_0 - \boldsymbol{u}(0) := 0. \tag{2.6}$$

$$\frac{\delta \mathscr{L}}{\delta c} = \frac{1}{2}\langle \boldsymbol{u}_0, \boldsymbol{u}_0\rangle - E_0 := 0. \tag{2.7}$$

First variations with respect to the physical variables yield a complementary set of adjoint equations,

$$\frac{\delta \mathscr{L}}{\delta \boldsymbol{u}} = \partial_t \boldsymbol{v} + N^\dagger(\boldsymbol{v}, \boldsymbol{u}) + \boldsymbol{\nabla} q + \left(\frac{\boldsymbol{u}}{E_0} - \boldsymbol{v}\right)\Big|_{t=T} + (\boldsymbol{v} - \boldsymbol{v}_0)\,|_{t=0} := 0, \tag{2.8}$$

$$\frac{\delta \mathscr{L}}{\delta p} = \boldsymbol{\nabla} \cdot \boldsymbol{v} := 0, \tag{2.9}$$

$$\frac{\delta \mathscr{L}}{\delta \boldsymbol{u}_0} = \boldsymbol{v}_0 - c\boldsymbol{u}_0 := 0. \tag{2.10}$$

Here,

$$N^\dagger(v_i, \boldsymbol{u}) := \partial_j\left(u_j v_i\right) - v_j \partial_i u_j + \partial_j\left(U_j v_i\right) - v_j \partial_i U_j + \frac{1}{Re}\partial_j \partial_j v_i \tag{2.11}$$

can be identified as the adjoint of N and $\boldsymbol{v}$, $\boldsymbol{v}_0$ and q are the adjoint variables of $\boldsymbol{u}$, $\boldsymbol{u}_0$ and p. Equation (2.8) is in reality three equations. The first part, $\partial_t \boldsymbol{v} + N^\dagger(\boldsymbol{v}, \boldsymbol{u}) + \boldsymbol{\nabla} q = \boldsymbol{0}$, must be satisfied at all times and are the adjoint Navier–Stokes equations. Since the full Navier–Stokes equations have been imposed, the adjoint operator depends on the velocity field $\boldsymbol{u}$. The sign of the diffusion term is also reversed and therefore the adjoint equation can only be solved backwards in time. The second part of (2.8), $(\boldsymbol{u}/E_0 - \boldsymbol{v})|_{t=T} = \boldsymbol{0}$, is a terminal condition, linking our physical and adjoint variables, and needs only to be satisfied at time T. The third part, $(\boldsymbol{v} - \boldsymbol{v}_0)|_{t=0} = \boldsymbol{0}$, is a condition linking $\boldsymbol{v}_0$ and $\boldsymbol{v}(0)$, which must be satisfied at $t = 0$.

We also choose to extend previous recent formulations (PK10; Cherubini *et al.* 2010, 2011*a*,*b*; M11; PWK12) and enable optimization over all possible choices of the target time T. The first variation with respect to T yields the simple relation

$$\frac{\partial \mathscr{L}}{\partial T} := \frac{1}{E_0}\frac{\mathrm{d}}{\mathrm{d}T}E(T) = 0, \tag{2.12}$$

provided $\boldsymbol{u}$ is incompressible and satisfies the Navier–Stokes equations at $t = T$. As discussed in § 1, this introduces a significant further complication to the identification of 'optimal' perturbations as the initial energy E_0 is increased. It is entirely possible that qualitatively different initial perturbations (with qualitatively different optimal time intervals) will dominate for different ranges of initial perturbation energy E_0, and so there is no necessity for the time interval T_{opt} associated with the optimal perturbation identified by our algorithm to be a continuous function of E_0.

Our target-time-optimization algorithm proceeds as follows. We first start with a suitable guess for the optimal initial condition, $\boldsymbol{u}_0$, and a target time T. We then time-march our initial condition to time T using the Navier–Stokes equations and use $(\boldsymbol{u}/E_0 - \boldsymbol{v})|_{t=T} = 0$ to 'initialize' the adjoint equations, which are then solved backwards in time to calculate $\boldsymbol{v}_0$. This procedure ensures that all the variational equations are satisfied apart from (2.10) and (2.12). If the current value for $\boldsymbol{u}_0$ is optimal then (2.10) will be satisfied: on the other hand, if (2.10) is not satisfied, it provides an estimate for the gradient $\delta\mathscr{L}/\delta\boldsymbol{u}_0$, i.e.

$$\frac{\delta \mathscr{L}}{\delta \boldsymbol{u}_0^{(n)}} \simeq \boldsymbol{g}^{(n)} = \boldsymbol{v}_0^{(n)} - c^{(n)}\boldsymbol{u}_0^{(n)}, \tag{2.13}$$

where the superscript denotes the nth iteration. We then update the initial condition using a method of steepest ascent by setting

$$\boldsymbol{u}_0^{(n+1)} = \boldsymbol{u}_0^{(n)} + \epsilon \boldsymbol{g}^{(n)} \tag{2.14}$$

(note that $\boldsymbol{u}_0^{(n+1)}$ is incompressible as $\boldsymbol{\nabla} \cdot \boldsymbol{g}^{(n)} = 0$), where $c^{(n)}$ is selected to impose the normalization condition explicitly, i.e.

$$\tfrac{1}{2}\langle \boldsymbol{u}_0^{(n+1)}, \boldsymbol{u}_0^{(n+1)} \rangle = E_0. \tag{2.15}$$

The parameter ϵ determines how big a 'step' we take after each iteration, and typically, we choose ϵ to be sufficiently small so that the gain increases monotonically with iteration, i.e.

$$G^{(n+1)} > G^{(n)}. \tag{2.16}$$

We find that if a condition of this form constraining the variation of gain from one iteration to the next is not imposed, the algorithm experiences very large fluctuations for $E_0 > E_{fail}$. Typically, ϵ varies by several orders of magnitude during a particular

sequence of iterations. Once a new value of $\boldsymbol{u}_0$ is obtained, T is updated by integrating the Navier–Stokes equations forward in time using the updated $\boldsymbol{u}_0$ as an initial condition until a maximum value of $E(t)$ is reached. The time of this maximum is taken as the new value of T_{opt} for this particular value of E_0 and (2.12) is then satisfied. Convergence of the procedure was assessed by examining how the normalized residual

$$R_n := \langle \delta\mathscr{L}/\delta\boldsymbol{u}_0^{(n)}, \delta\mathscr{L}/\delta\boldsymbol{u}_0^{(n)}\rangle / \langle \boldsymbol{v}_0^{(n)}, \boldsymbol{v}_0^{(n)}\rangle, \tag{2.17}$$

at the nth iteration, behaved as n increased.

3. BF92 geometry

The underlying objective of this paper is to investigate how optimal initial conditions for energy growth over a finite time interval T change as a function of E_0. We are interested in three particular core issues: the role played by the finite-amplitude manifestations of the optimal perturbations of the underlying strictly linear optimization problem (i.e. the perturbations we refer to as belonging to the QLOP_T solution branch) as E_0 increases towards E_{fail}; whether it is possible to identify, for sufficiently long optimization time intervals, the special 'final' nonlinear optimal perturbations (which we refer to as the $\mathrm{NLOP}_T^{(f)}$ solution branch) which converge towards the minimal seed as E_0 approaches E_c from below; and whether we can find evidence, either direct or indirect, that suggests that the $\mathrm{NLOP}_T^{(f)}$ are convergent solutions to our optimization problem for all energies less than but sufficiently close to E_c, thus suggesting that $E_{fail} = E_c$. To investigate these issues, we present results for the geometry studied previously in the linear regime ($E_0 \to 0$) in BF92: a periodic box with dimensions $L_x = 2\pi/0.49 = 13.66$, $L_y = 2$ and $L_z = 2\pi/1.9 = 3.31$ (or $4.08\pi \times 2 \times 1.05\pi$) with $Re = 1000$. We use a modified version of the Diablo CFD solver (Taylor 2008), which is spectral in x and z and finite-difference in y, to solve the forward and adjoint equations as described in the previous section.

3.1. *The quasi-linear optimal perturbation*

For sufficiently small initial energies E_0, a resolution of $128 \times 256 \times 32$ in x, y and z respectively and time step $\Delta t = 0.025$, we found that the optimal perturbation resembled that previously reported (see BF92 for more details) linear optimal perturbation in both gain and structure, justifying our identification of this perturbation as a 'quasi-linear optimal perturbation' (QLOP_T). As noted by BF92, the form of the initial perturbation and its time evolution vary relatively little with the particular length of the optimization time interval T, provided the optimization interval is sufficiently long. The peak value of the gain for this particular optimal perturbation is approximately 1100, and occurs for an optimization interval $T = T_Q \simeq T_L = 125.25$ (in units of h/U). With increasing but still small E_0, the peak gain and globally optimal time horizon $T = T_Q$ of the QLOP_{T_Q} remains close to constant (i.e. $T_L = T_Q = T_{opt}$ as shown in figure 3*a,b*).

However, beyond a certain energy threshold (approximately $2.2 \times 10^{-6} < E_{fail} < 2.25 \times 10^{-6}$), there is a sudden and large jump in the gain achievable, as shown in figure 3(*a*), and the associated optimal time tends to very large values as E_0 approaches this threshold energy from above. As discussed in the following subsection, the initial conditions found by our algorithm for these values of $E_0 \geqslant E_{fail}$ evolve into turbulent states, and our algorithm fails to converge. The observed decrease in gain as E_0 increases above this threshold energy E_{fail} (figure 3*a* indicates $G \sim 1/E_0$) suggests

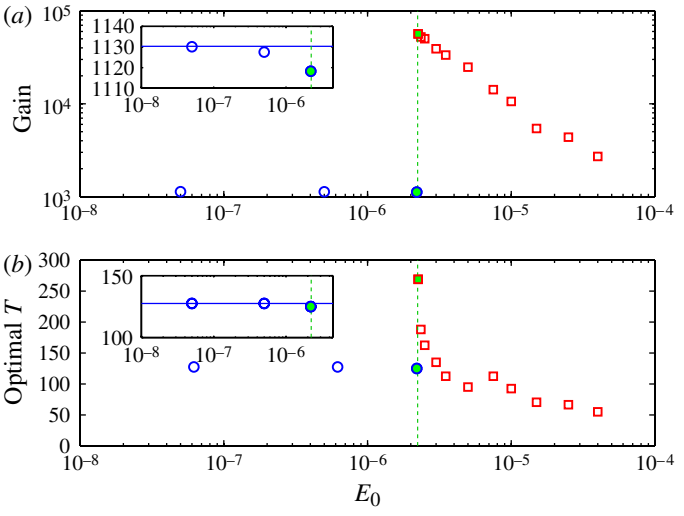

FIGURE 3. (Colour online) Variation with initial energy E_0 of (*a*) the gain $G(T) = E(T)/E_0$ and (*b*) the globally optimal time T_{opt} for the BF92 flow geometry. The critical energy $2.2 \times 10^{-6} < E_c < 2.25 \times 10^{-6}$, where T_{opt} jumps markedly, is indicated by a vertical green dashed line. In the insets, the gain (1130) and T_{opt} (125.25) for the underlying linear problem are marked with a horizontal blue solid line. Blue circles mark the properties of $\mathrm{QLOP}_{T_{opt}}$ (i.e. $T_Q = T_{opt}$), while the red squares mark the properties of turbulent seeds. The filled circle corresponds to $\mathrm{QLOP}_{T_{opt}}$ for $E_0 = 2.2 \times 10^{-6}$ shown in figure 4 and in figures 5(*a*) and 6(*a*), while the filled square corresponds to the 'critical' T_c turbulent seed for $E_0 = 2.25 \times 10^{-6}$ shown in figure 4 and in figures 5(*c*) and 6(*c*).

that the saturated energy for these perturbations is approximately constant, or at least largely insensitive to the value of E_0, provided $E_0 > E_{fail}$, which is consistent with a (turbulent) attractor being reached. These results suggest that the critical energy E_c for turbulence to be accessible satisfies $E_c \lesssim E_{fail}$. It is also apparent that the behaviour of the optimal time T_{opt} associated with the maximum gain over all possible time horizons is entirely consistent with the schematic picture shown in figure 2(*a*) and described in detail in § 1: the $\mathrm{QLOP}_{T_{opt}}$ (shown by the thick black line in the figure) 'masks' the potential presence of the final nonlinear optimal perturbation $\mathrm{NLOP}_T^{(f)}$, which is conjectured to converge to the turbulent seed for all $E_0 < E_c$. As the initial energy amplitude E_0 approaches E_{fail} from below, the $\mathrm{QLOP}_{T_{opt}}$ remains dominant, with gain (and optimal time) very similar to the values from the linear problem.

There is strong evidence that the algorithm converges straightforwardly to this perturbation from a range of initial conditions for all values of $E_0 < E_c$. Figure 4(*a*) plots the normalized residual R_n against iteration n for the $\mathrm{QLOP}_{T_{opt}}$ at $E_0 = 2.2 \times 10^{-6}$, whose gain $G(T)$ and optimal time T_{opt} are marked with filled blue circles in figure 3. For the calculation shown in figure 4, we use random noise as an initial guess, which gives rise to the relatively large initial value of the normalized residual R_n (for $n \leqslant 5$). The observation that R_n drops so strongly (by fifteen orders of magnitude) while the gain rapidly asymptotes to a specific value (1118) very close to the value (1130) for the underlying linear problem, lends credibility to the assertion that our algorithm is converging to this optimal perturbation. Rerunning the procedure for a further five randomly chosen initial conditions reproduces the same result. We also saw similarly

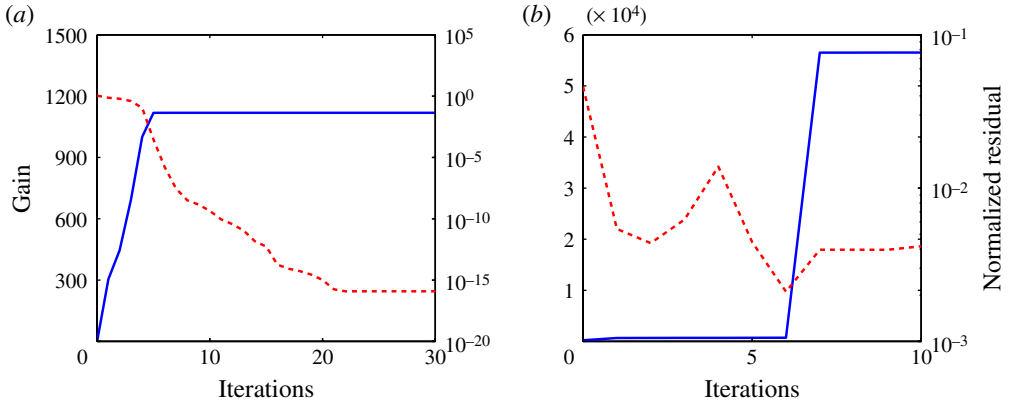

FIGURE 4. (Colour online) Gain $E(T)/E_0$ (blue solid line) and R_n (as defined in (2.17) and plotted with a red dashed line) plotted against iteration for (*a*) the $\mathrm{QLOP}_{T_{opt}}$ at $E_0 = 2.2\times10^{-6}$ where the gain is 118, and (*b*) the critical T_c turbulent seed with $E_0 = 2.25 \times 10^{-6}$ where the gain is $G > 5.6 \times 10^4$.

strong convergence for all the other perturbations on the $\mathrm{QLOP}_{T_{opt}}$ solution branch with $E_0 < 2.2 \times 10^{-6}$.

In fact, it is possible to converge to the $\mathrm{QLOP}_{T_{opt}}$ solution branch for $E_c < E_0 \lesssim 2E_c$ if the initial guess for the algorithm is chosen sufficiently closely to the $\mathrm{QLOP}_{T_{opt}}$, demonstrating that it persists as a local maximum in (optimal) solution space for a wide range of initial energies. Our identification of this perturbation as being closely related to the linear optimal perturbation can be confirmed by consideration of its spatial and temporal structure. In figures 5(*a*) and 6(*a*), we plot contours and isosurfaces of streamwise velocity u at various times. These images clearly show the expected streamwise-aligned and spanwise-periodic streak structure characteristic of the linear optimal perturbation as identified by BF92.

3.2. *Turbulent seeds*

As is apparent in figure 3, when the initial energy E_0 crosses the threshold value E_{fail}, both the globally optimal time T_{opt} and the gain increase to values very much larger than those associated with the linear problem. There is clearly a disconnect between the perturbations identified by our algorithm either side of this threshold energy. Therefore, in this flow geometry, optimizing perturbations over all possible time horizons does not address the validity of the conjectures of PWK12, showing that this flow is qualitatively different from the pipe flow which they considered. In particular, it is clear that $T \simeq T_L = 125$ is not sufficiently 'long' to allow the testing of their conjectures.

However, it is possible to establish that the threshold energy we have identified may be interpreted as being the energy E_{fail} at which our algorithm fails to converge, and also that for initial energies greater than this threshold the initial perturbations may be thought of as 'turbulent seeds', since they trigger transition eventually. We show the generic behaviour of our algorithm for perturbations with $E_0 > E_{fail}$ in figure 4(*b*), for the special 'critical' T_c perturbation with $E_0 = 2.25 \times 10^{-6}$ shown with a filled red square in figure 3. Although the gain apparently saturates at a substantially elevated value compared to $\mathrm{QLOP}_{T_{opt}}$ at $E_0 = 2.2 \times 10^{-6}$ in figure 4(*a*), the normalized

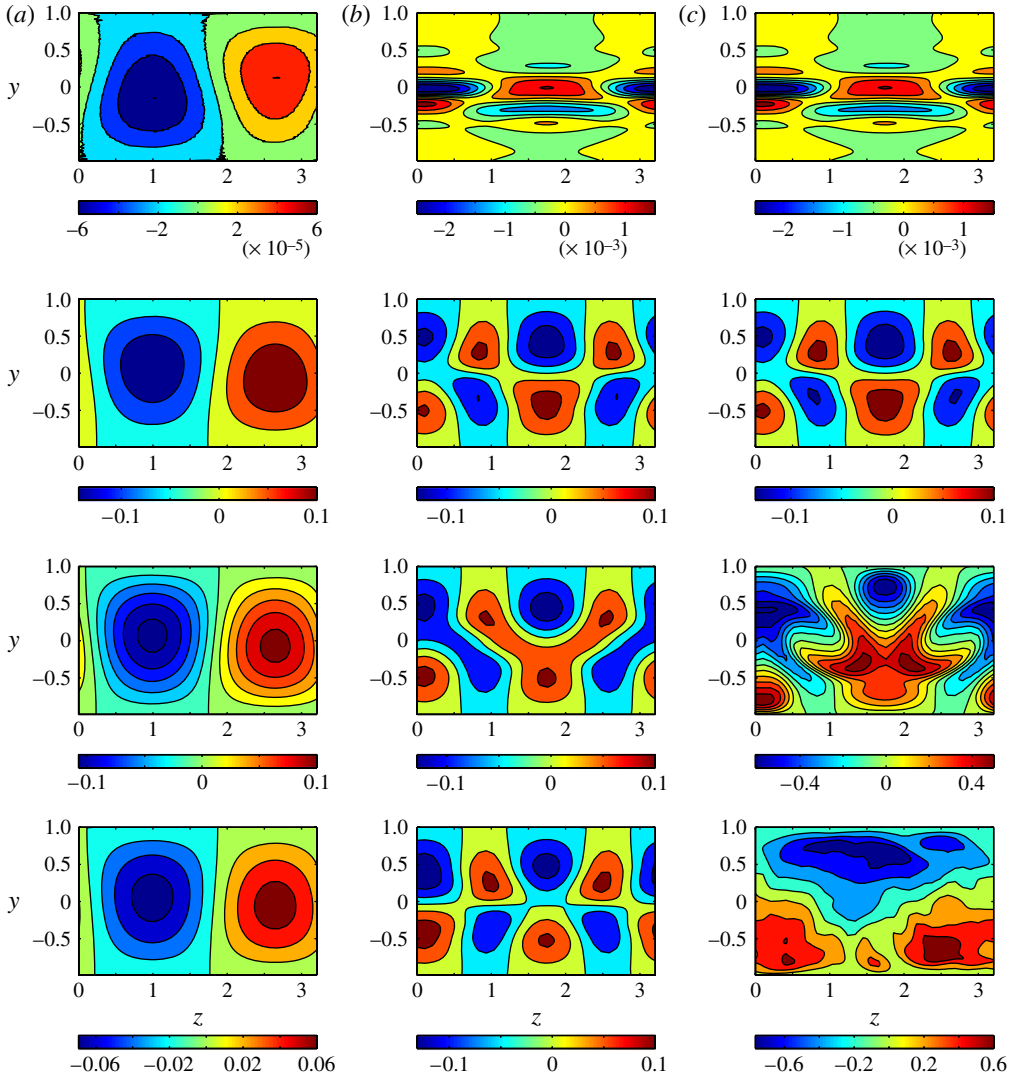

FIGURE 5. Contours of streamwise velocity u at times 0, 150, 250, 350 for (a) QLOP$_{T_{opt}}$ with $E_0 = 2.2 \times 10^{-6}$, (b) the edge state calculated by using the conventional bisection approach with $E_0 \simeq E_c$, and(c) the 'critical' T_c turbulent seed for $E_0 = 2.25 \times 10^{-6} \gtrsim E_c$. Contour levels, from top to bottom, are: (a) (min, spacing, max) $= (-6, 2, 6) \times 10^{-5}$, $(-0.1, 0.05, 0.1)$, $(-0.1, 0.02, 0.1)$, $(-0.06, 0.02, 0.06)$; (b) (min, spacing, max) $= (-2, 0.5, 1.5) \times 10^{-3}$ and $(-0.1, 0.05, 0.1)$ subsequently; (c) (min, spacing, max) $= (-2, 0.5, 1.5) \times 10^{-3}$, $(-0.1, 0.05, 0.1)$, $(-0.6, 0.1, 0.5)$, $(-0.6, 0.2, 0.6)$.

residual R_n as defined in (2.17) does not drop to small values, suggesting highly non-smooth properties of the solution space, which would be expected to occur when the flow can become turbulent. This figure also shows that the gain jumps during one iteration, indicative of suddenly finding a 'turbulent' end state. The residual remains relatively high, and in fact it proves very difficult to continue the iteration. This suggests that there are several turbulent seeds for this initial energy, and so $E_0 = 2.25 \times 10^{-6}$ should be considered as an upper bound on E_c.

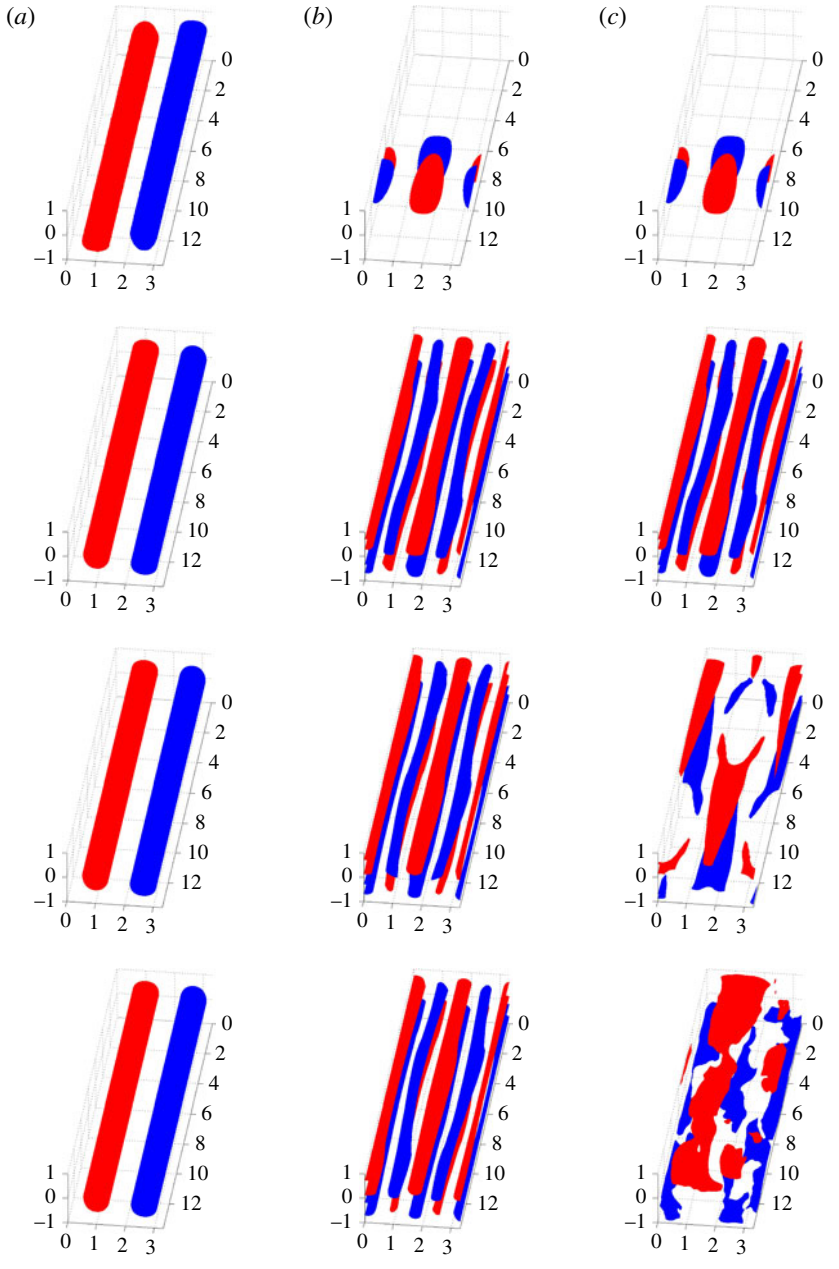

FIGURE 6. (Colour online) Isosurfaces of streamwise velocity u, at 60 % of maximum and minimum values, at times 0, 150, 250, 350, for (a) QLOP$_{T_{opt}}$ with $E_0 = 2.2 \times 10^{-6}$, where the amplitude is decaying for the lower three panels, (b) the edge state calculated by using the conventional bisection approach with $E_0 \simeq E_c$, and (c) the T_c turbulent seed above the edge at $E_c < E_0 = 2.2 \times 10^{-6}$.

The next natural question to consider is whether this threshold energy E_{fail} can also be identified with the critical energy for an initial condition to lead to turbulence, i.e. if $E_{fail} = E_c$ the initial energy of the minimal seed. In figures 5(c) and 6(c), at the same

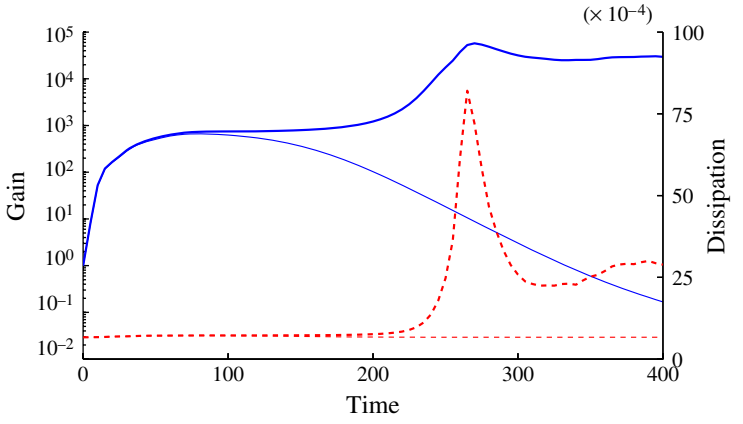

FIGURE 7. (Colour online) Time variation of the gain $G(t) = E(t)/E_0$ (plotted with a thick blue solid line) and dissipation rate (thick red dashed line) for the critical T_c turbulent seed with $E_0 = 2.3 \times 10^{-6}$. For comparison we have also plotted the time variation of the gain (thin blue solid line) and dissipation rate (thin red dashed line) associated with a perturbation with the same initial structure as the T_c turbulent seed but with rescaled initial energy of $E_0 = 2.2 \times 10^{-6}$.

times as for the $\mathrm{QLOP}_{T_{opt}}$ at $E_0 = 2.2 \times 10^{-6}$ (marked by a filled blue circle in figure 3 and shown in the left-hand panels), we plot contours and isosurfaces of the streamwise velocity of the flow evolving from the critical 'optimal' T_c perturbation identified by our algorithm with $E_0 = 2.25 \times 10^{-6}$, and marked with a filled red square in figure 3. Three characteristics are immediately apparent. Firstly, the initial structure of this T_c perturbation is qualitatively different from the $\mathrm{QLOP}_{T_{opt}}$, with the T_c perturbation showing strong initial spatial localization. Secondly, as time passes, this localized T_c perturbation 'unpacks' and extends throughout the computational domain, with an appreciably smaller spanwise scale than the evolving $\mathrm{QLOP}_{T_{opt}}$ perturbation. This 'unpacking' leads to enhanced energy gain through a combination of the well-known Orr and lift-up mechanisms (see PWK12 and Cherubini *et al.* 2010, 2011*b*). Finally, for $t > 200$, when $\mathrm{QLOP}_{T_{opt}}$ is already starting to decay and the flow is relaminarizing, the T_c perturbation breaks down (through a streak instability, e.g. Reddy *et al.* 1998), and indeed appears to undergo a transition to turbulence, justifying our identification of this initial perturbation as a turbulent seed.

We present further evidence that the T_c perturbation is a turbulent seed in figure 7, where we plot the time-varying gain (with a thick blue solid line) and instantaneous dissipation rate (with a thick red dashed line) of the evolving flow for the T_c perturbation with $E_0 = 2.25 \times 10^{-6}$. For comparison, we plot the same quantities (with thin lines) for an evolving flow with an initial perturbation of the same spatial structure as the T_c perturbation, whose amplitude is uniformly rescaled so that the initial energy of the perturbation is 2.2×10^{-6}, i.e. just below the critical threshold energy E_{fail} shown in figure 3. Initially, the evolution of the two flows is very similar. The dissipation rate remains at a small, essentially laminar value, while the gain grows substantially, and reaches a plateau, corresponding to a gain of approximately 650. Importantly, and consistently with the schematic picture presented in figure 2(*a*), this plateau is substantially below the maximum attained by the $\mathrm{QLOP}_{T_{opt}}$ perturbation (1118) with similar initial energy at time $T_Q = T_{opt} = 125$.

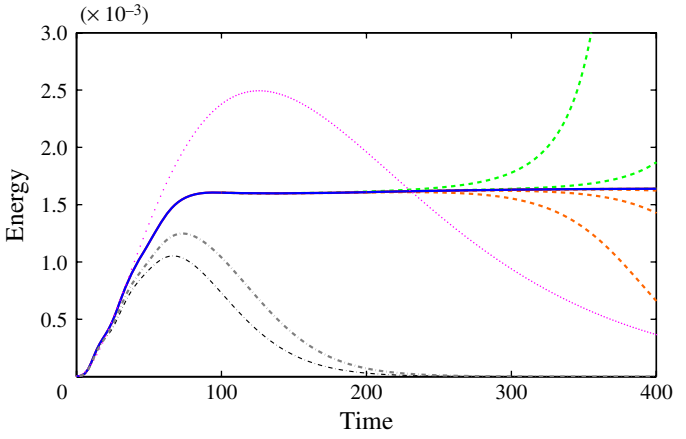

FIGURE 8. (Colour online) Perturbation energy against time for various initial states close to the edge in the BF92 geometry. Every 100 time units, the edge state is rescaled to produce new upper and lower bounds, and its energy is plotted with a solid blue line. The dashed (upper) green and (lower) orange lines plot the continued time evolution of bracketing solutions as they are considered to no longer be on the edge. The QLOP_{300} with $E_0 = 2.23205 \times 10^{-6}$, and shown in figure 9(*a*), is plotted with a magenta dotted line. The initial perturbation identified as the final $\mathrm{NLOP}^{(f)}_{300}$ with $E_0 = 2.2305 \times 10^{-6}$ and shown in figure 9(*b*) is plotted with the first divergent dashed orange line. The associated initial perturbations identified as the final $\mathrm{NLOP}^{(f)}_{100}$ with $E_0 = 2.1 \times 10^{-6}$ and the final $\mathrm{NLOP}^{(f)}_{50}$ with $E_0 = 2.0 \times 10^{-6}$ and shown in figure 9(*b,c*) are plotted with a thick grey dot-dashed line and a thin black dot-dashed line respectively.

However, at sufficiently late times $t > 200$ the behaviour of the two perturbations starts to diverge markedly. The rescaled perturbation with energy below the threshold energy decays, and the flow is clearly relaminarizing with the dissipation rate remaining at a very small value. Conversely, the T_c perturbation increases enormously in magnitude from the intermediate plateau value to a maximum gain $G > 5.6 \times 10^4$ at a time $T_{opt} = 270$, associated with a very large spike in dissipation rate. Subsequently the dissipation rate stays at an enhanced level, indicating that turbulence has been reached and therefore that the threshold energy marked in figure 3 is close to the critical energy E_c. This behaviour also suggests that it would be appropriate to consider an optimization problem with an adequately long fixed time horizon of $T = 300$, to investigate the existence (or otherwise) of the 'final' nonlinear optimal perturbation $\mathrm{NLOP}^{(f)}_T$ solution branch, which is conjectured to converge to the minimal seed as $E_0 \to E_c^-$.

3.3. *The 'final' nonlinear optimal perturbation* $\mathrm{NLOP}^{(f)}_T$

In the conceptual picture presented by PWK12, one unique initial condition to trigger turbulence – the minimal seed – should emerge as the limiting state of a specific, convergent nonlinear optimal perturbation (herein referred to as the 'final' $\mathrm{NLOP}^{(f)}_T$) as $E_0 \to E_c^-$, and this minimal seed is the lowest accessible energy state on the laminar–turbulent 'edge'. To investigate this further, we first refine our estimate for E_c by following the well-established procedure for 'edge-tracking' (Itano & Toh 2001; Skufca *et al.* 2006; Schneider *et al.* 2007; Duguet *et al.* 2008). The turbulent seed discussed above is successively rescaled until it stays close to the 'edge' for a large

time of $t = 400$. Figure 8 makes it clear that the edge state (attracting state for edge-confined dynamics) has an approximately constant energy of $E = 1.6 \times 10^{-3}$. This is consistent with the work of Schneider *et al.* (2008), who treat a PCF system $4\pi \times 2 \times 2\pi$, albeit at $Re = 400$, and find a steady edge state. From this calculation, we obtain the refined estimate that $2.23205 \times 10^{-6} < E_c < 2.2321 \times 10^{-6}$. The need to consider sufficiently long optimization intervals is illustrated clearly by the behaviour of the quasi-linear optimal perturbation for the fixed optimization interval $T = 300$ with initial energy $E_0 = 2.23205 \times 10^{-6}$. This QLOP_{300} behaves in an essentially identical manner to the $\mathrm{QLOP}_{T_{opt}}$ discussed above, reaching a maximum gain substantially larger than the intermediate plateau of the edge state at $T \simeq 130$, before decaying, such that the gain at the target time $T = 300$ is below that of the plateau, and has $G(300) \simeq 400$. Therefore, the final nonlinear optimal perturbation, which is conjectured to converge to the minimal seed, is expected to have larger gain than the QLOP_{300} when $T = 300$ but not for substantially smaller optimization intervals.

It is important to remember that our algorithm is in fact only able to identify local maxima in the growth rate of perturbations, and so the particular form of the 'optimal perturbation' may well be sensitive to the choice of the initial guess for the initial perturbation structure we use to start the algorithm. In particular, it is possible for us still to converge to the QLOP_{300} even when its gain is below that of the $\mathrm{NLOP}_{300}^{(f)}$ for initial energies very close to E_c. In figure 9(*a*), we plot the gain and normalized residual (as defined in (2.17)) R_n against iteration for the QLOP_{300} with $E_0 = 2.2 \times 10^{-6}$. As for the QLOP_T calculation shown in figure 4, we use random noise as an initial guess, explaining the initial relatively large value of the normalized residual R_n defined in (2.17), and clearly are able to obtain strong convergence to this local maximum in gain $G(300) = 421$.

However, over this time interval, and for E_0 sufficiently close to E_c, the gain of the inherently nonlinear optimal perturbation which approaches very close to the edge state for a substantial time (plotted as the first divergent dashed orange line in figure 8) is expected to be substantially larger than that of the QLOP_{300}. Therefore, for initial 'guesses' chosen sufficiently closely to those which evolve into the edge state, we should be able to identify the 'final' nonlinear optimal perturbation $\mathrm{NLOP}_T^{(f)}$ solution branch. Our algorithm is indeed able to identify such an initial perturbation, although when E_0 is very close to E_c, the algorithm does not show very good convergence properties. Increasing the cross-stream resolution substantially (so the total resolution is now $128 \times 1536 \times 32$) improves matters but does not eliminate the difficulty. In figure 9(*b*), we plot the gain and normalized residual (as defined in (2.17)) R_n against iteration for what we believe to be the $\mathrm{NLOP}_{300}^{(f)}$ with $E_0 = 2.23025 \times 10^{-6}$ and the higher resolution of $128 \times 1536 \times 32$ in the x, y and z directions and $\Delta t = 0.1$. For this iteration, and the other iterations investigating the $\mathrm{NLOP}^{(f)}$ solution branch shown in figure 9(*c*,*d*), we relaxed the condition on the monotonicity of the gain (2.16) to

$$G^{(n+1)} > 0.95 G^{(n)}, \tag{3.1}$$

which slightly improved the initial convergence properties.

The gain clearly tends to a fixed value just below 700, and the normalized residual R_n is really quite small (approximately $R_n = 3.5 \times 10^{-6}$) but fails to reduce further, for reasons we do not understand. The initial structure and time evolution of this perturbation is essentially indistinguishable from those of the edge state shown in figures 5(*b*) and 6(*b*). The initial structure is spatially localized in a very similar way

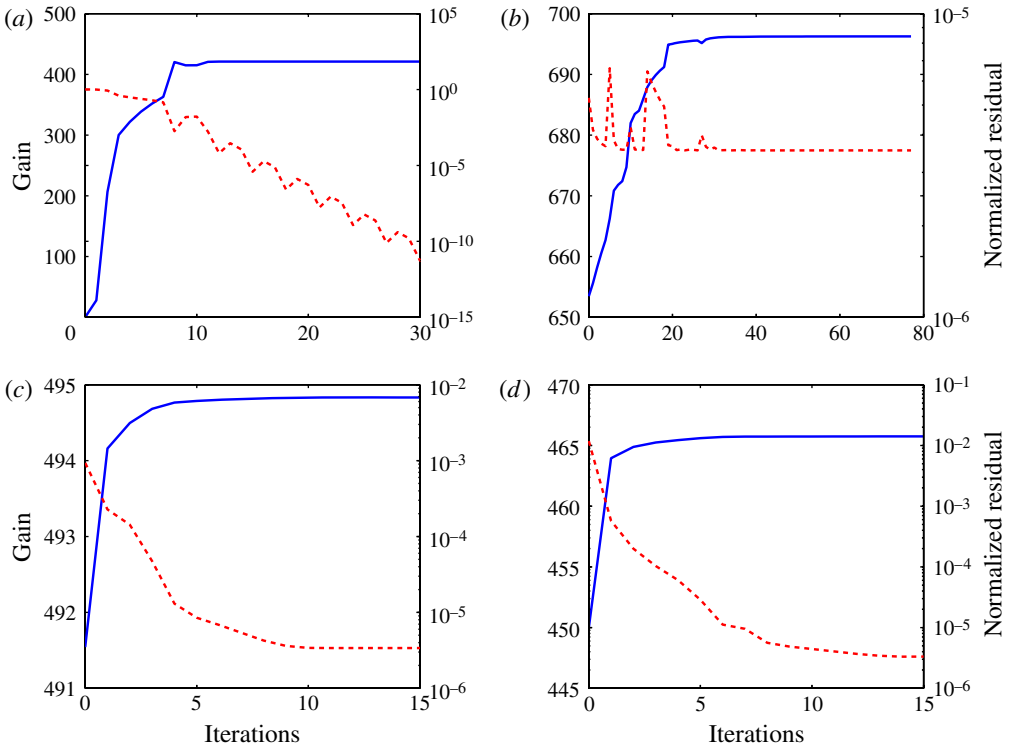

FIGURE 9. (Colour online) Gain $E(T)/E_0$ (blue solid line) and normalized residual R_n (as defined in (2.17) and plotted with a red dashed line) plotted against iteration. (*a*) The QLOP_{300} with $E_0 = 2.2 \times 10^{-6}$, with resolution $128 \times 256 \times 32$ in the x, y and z directions and $\Delta t = 0.025$, showing an ultimate gain of 421. (*b*) The $\mathrm{NLOP}^{(f)}_{300}$ with $E_0 = 2.23025 \times 10^{-6}$, with resolution $128 \times 1536 \times 32$ in the x, y and z directions and $\Delta t = 0.1$ showing an ultimate gain of 696. (*c*) The $\mathrm{NLOP}^{(f)}_{100}$ with $E_0 = 2.1 \times 10^{-6}$, with resolution $128 \times 1536 \times 32$ in the x, y and z directions and $\Delta t = 0.1$ showing an ultimate gain of 495. (*d*) The $\mathrm{NLOP}^{(f)}_{50}$ with $E_0 = 2.0 \times 10^{-6}$, with resolution $128 \times 1536 \times 32$ in the x, y and z directions and $\Delta t = 0.1$ showing an ultimate gain of 466.

to the critical T_c turbulent seed shown in the right-hand panels, and the perturbation also 'unpacks' in the same way along the streamwise extent of the computational domain, growing through a combination of the Orr and lift-up mechanisms. However, similar to the time evolution of the rescaled perturbation whose evolution is shown in figure 7, the amplitude is just too small to trigger turbulence, and the perturbation approaches a steady quasi-periodic structure, with essentially constant perturbation amplitude over a very long time interval.

The initial guess which we choose for this perturbation is the initial perturbation which we have identified as the minimal energy state (the minimal seed) of the edge state scaled to be just slightly smaller than the critical energy E_c for the onset of turbulence. This guess is actually very close to the local optimal choice, as is evidenced by the relatively small value of the normalized residual for the first iterations. Unfortunately, since the residual does not drop much further, it is hard to claim convergence. If it had been possible to start further away, the drop to a residual of $O(10^{-6})$ would be more convincing of convergence (the fact that the normalized

residual saturates is consistent with the observations of PWK12 and is not currently understood).

As the initial energy E_0 decreases from E_c, even locally optimal perturbations cease to follow the time evolution of the minimal seed, and 'drop off' the edge, decaying and relaminarizing at earlier and earlier times. There is a minimum initial energy $E_0 = E_f$ at which initial perturbations will no longer approach the edge at all, a stage at which we would consider the 'final' nonlinear perturbation ($\mathrm{NLOP}^{(f)}$) solution branch not to exist. To demonstrate the existence of this solution branch, we therefore reduce the optimization time horizon as we reduce E_0 to identify locally optimal perturbations with similar initial structure to the minimal seed, and thus to the $\mathrm{NLOP}^{(f)}_{300}$ discussed above. The reduced optimization time horizon allows us to consider the perturbation's gain at least close to its maximum (across all time) value, thus maximizing the chances for our algorithm to converge to this solution branch as $E_0 \to E_f^+$. The time evolution of the energy of two such perturbations is plotted in figure 8. When $E_0 = 2.1 \times 10^{-6}$ (i.e. $E_0 \simeq 0.94E_c$) we consider a fixed optimization time interval of $T = 100$. We plot with a grey dot-dashed line the time evolution of the energy of a locally optimal perturbation, with an initial 'guess' of the $\mathrm{NLOP}^{(f)}_{300}$, which clearly continues to trace, at least initially, the temporal evolution of the minimal seed. Similarly, when $E_0 = 2.0 \times 10^{-6}$ (i.e. $E_0 \simeq 0.90E_c$) we consider an even shorter fixed optimization time interval of $T = 50$, and plot the equivalent time evolution with a black dot-dashed line. For both of these optimization problems, we use consistently the higher resolution of $128 \times 1536 \times 32$ in the x, y and z directions and $\Delta t = 0.1$.

Since the initial structure of these perturbations is extremely similar to the $\mathrm{NLOP}^{(f)}_{300}$ (and indeed the minimal seed) we identify these two perturbations as part of the same 'final' nonlinear optimal perturbation solution branch, and hence label them as the $\mathrm{NLOP}^{(f)}_{100}$ and $\mathrm{NLOP}^{(f)}_{50}$ respectively. Also, because these perturbations have initial energy slightly further away from the critical value of E_c than the $\mathrm{NLOP}^{(f)}_{300}$, we are now able to demonstrate somewhat better convergence properties for our algorithm. In figures 9(*c*) and 9(*d*) respectively, we plot the gain and normalized residual R_n against iteration for the $\mathrm{NLOP}^{(f)}_{100}$ with $E_0 = 2.1 \times 10^{-6}$ and the $\mathrm{NLOP}^{(f)}_{50}$ with $E_0 = 2.0 \times 10^{-6}$ (which we believe is a good estimate for the minimum energy E_f at which this solution branch exists). In both cases, the gain appears to be approaching a saturated value, of 495 for the $\mathrm{NLOP}^{(f)}_{100}$ and 466 for the $\mathrm{NLOP}^{(f)}_{50}$ respectively. Since the initial guesses are further away from the final 'optimal' perturbation than in the $\mathrm{NLOP}^{(f)}_{300}$ calculation, the normalized residual drops substantially with iterations giving better evidence for convergence, although again R_n appears to saturate at $O(10^{-6})$.

It is important to reiterate that these perturbations are only locally optimal, as over these time horizons, the quasi-linear optimal perturbation solution branch (whose energy evolution is plotted with a dotted magenta line in figure 8) definitely has larger gain. However, for sufficiently close initial guesses, both in structure and in original energy E_0, to the critical T_c turbulent seed, we believe that we have obtained convincing evidence for the existence of the 'final' nonlinear optimal perturbation, which converges to the minimal seed as $E_0 \to E_c^-$. This suggests that, within the nomenclature of the conjectures of PWK12 discussed in § 1, $E_{fail} = E_c$.

Indeed, in this geometry and at this Re, there is strongly suggestive evidence consistent with both conjectures of PWK12, provided the optimization problem has a sufficiently long (and fixed) time interval. Specifically, the threshold energy for our algorithm to fail to converge corresponds to the critical energy $E_{fail} = E_c$ where a

minimal seed can be found. Turbulence transition can occur for small perturbations above this minimal seed, and there is a well-defined nonlinear optimal perturbation (which we refer to as the 'final' $\mathrm{NLOP}_T^{(f)}$ for $T = 300$) which converges to the minimal seed as $E_0 \to E_c^-$. However, in the BF92 geometry, for all energies $E_0 < E_c$, the finite-amplitude optimal perturbation (which we refer to as the $\mathrm{QLOP}_{T_{opt}}$) associated with the linear optimal perturbation always has a larger gain than the 'final' $\mathrm{NLOP}_T^{(f)}$ for all T. Therefore, for this flow geometry, the behaviour is as shown schematically in figure 2(*a*). In the next section, we consider the different PCF geometry discussed in M11, both to see if the behaviour is different again, and to investigate whether E_c depends on the particular form of the optimization problem being considered.

4. M11 geometry

In this section we examine a second, larger geometry of dimensions $4\pi \times 2 \times 2\pi$ (essentially twice as wide as that in BF92) at a higher Reynolds number $Re = 1500$, as considered in M11. Typically, we choose a resolution of $128 \times 288 \times 64$ in the x, y and z directions respectively, and a time step $\Delta t = 0.025$. Choosing the geometry and Reynolds number used by M11 has the specific benefit that we can compare our results to those obtained for a completely different optimization problem. As discussed in § 1, M11 optimized the total dissipation over a long time interval ($T = 300$) rather than the energy gain achieved at a specific target time.

Following the same approach as described in the previous section, and so optimizing the energy gain $G(T) = E(T)/E_0$ over all possible target times T, we once again find a threshold energy E_{fail} at which the gain and optimal time interval T_{opt} jumps markedly, and our algorithm ceases to converge. We believe, as in the BF92 geometry, that this threshold energy can be identified with the critical energy for the onset of turbulence and is found to be $3.2 \times 10^{-7} < E_{fail} = E_c < 3.25 \times 10^{-7}$, plotted as a vertical dashed line in figure 10(*a*,*b*). This particular value agrees well with M11, who found $3 \times 10^{-7} < E_c < 4 \times 10^{-7}$ (see their figure 1). (Note that ϵ_0 in M11 is E_0 here, as $\| \quad \|_E$ in their equation (1) is strictly a kinetic norm with a 1/2 included Monokrousos, personal communication.) Our calculated time for transition at $E_0 = 4.0 \times 10^{-7}$ is approximately 200, not too dissimilar from the transition time of 150 in M11. This suggests strongly that the particular choice of optimizing functional is not important for the calculation of a minimal seed, or more accurately to identify the critical energy E_c, provided the functional attains heightened values for turbulent flows (as discussed in PWK12).

Furthermore, we find that the behaviour of the identified optimal perturbations as E_0 increases from small values towards E_c is actually qualitatively different from that which we identified for the BF92 geometry. Figure 10(*a*) indicates that there are now three different energy intervals in this geometry rather than the two in BF92. As before, below a certain initial energy value $E_0 < E_1$ the $\mathrm{QLOP}_{T_{opt}}$ is selected, and above a critical energy $E_0 > E_c$ turbulent seeds with initial conditions significantly different from the $\mathrm{QLOP}_{T_{opt}}$ trigger turbulence. Between these two limiting energy ranges, however (i.e. for $E_1 < E_0 < E_c$), there now exists an intermediate range of initial energies where our algorithm generates an initial condition different from the QLOP_{T_Q}, in the sense that it displays localization in the cross-stream (y) direction, as well as a strong streamwise (x) variation as shown in figure 11. Using the nomenclature described in § 1, we call this qualitatively different optimal perturbation an $\mathrm{NLOP}_{T_{opt}}^{(1)}$, after PK10 and PWK12. Perturbations on this intermediate solution

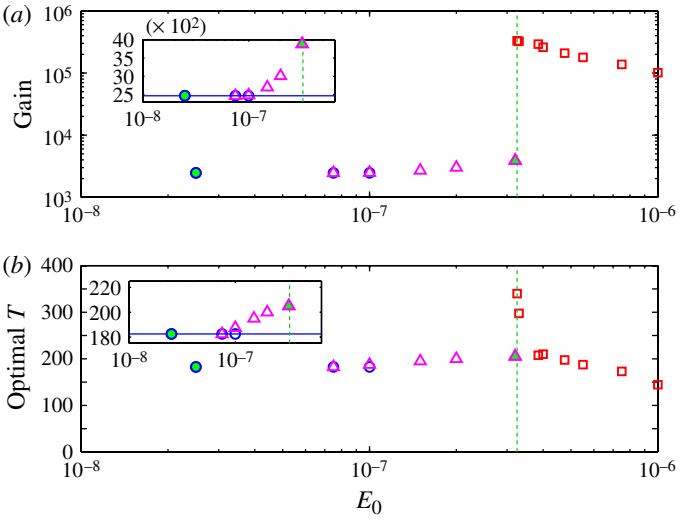

FIGURE 10. (Colour online) Variation with initial energy E_0 of (*a*) the gain $G(T) = E(T)/E_0$ and (*b*) the globally optimal time T_{opt} for the M11 flow geometry. The critical energy $3.2 \times 10^{-7} < E_c < 3.25 \times 10^{-7}$, where T_{opt} jumps markedly, is indicated by a vertical green dashed line. In the insets, the gain (2469) and T_{opt} (182.5) for the underlying linear problem are marked with a horizontal blue solid line. Blue circles mark the properties of $\mathrm{QLOP}_{T_{opt}}$ (i.e. $T_Q = T_{opt}$), while the red squares mark the properties of turbulent seeds and the magenta triangles mark the properties of the inherently nonlinear $\mathrm{NLOP}^{(1)}_{T_{opt}}$ solution branch. The cross-over time E_1, at which the $\mathrm{NLOP}^{(1)}_{T_{opt}}$ solution branch becomes apparently globally optimal, is approximately $E_1 \simeq 7.5 \times 10^{-8}$. The filled circle corresponds to the $\mathrm{QLOP}_{T_{opt}}$ with $E_0 = 2.5 \times 10^{-8}$ shown in figures 11–12, while the filled triangle corresponds to $\mathrm{NLOP}^{(1)}_{T}$ at $E_0 = 3.2 \times 10^{-7}$ shown in figures 11–14.

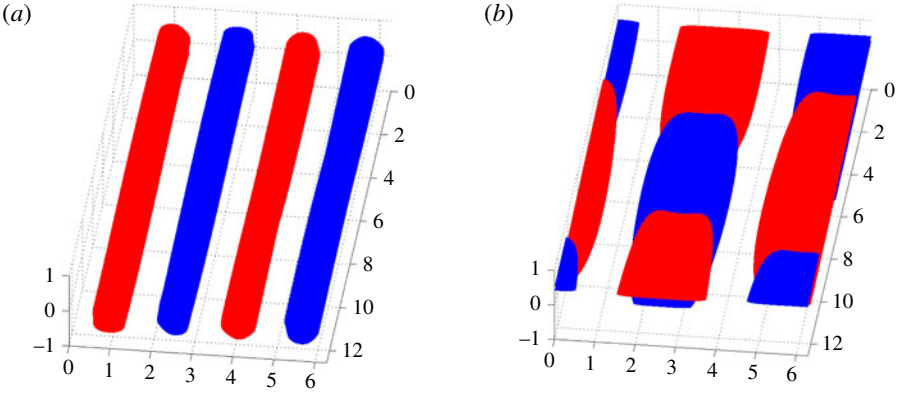

FIGURE 11. (Colour online) Isosurfaces of streamwise velocity u, at 60 % of maximum and minimum values, for (*a*) the $\mathrm{QLOP}_{T_{opt}}$ at $E_0 = 2.5 \times 10^{-8}$, marked with a filled blue circle in figure 10, and (*b*) the $\mathrm{NLOP}^{(1)}_{T_{opt}}$ at $E_0 = 3.2 \times 10^{-7}$, marked with a filled magenta triangle in figure 10.

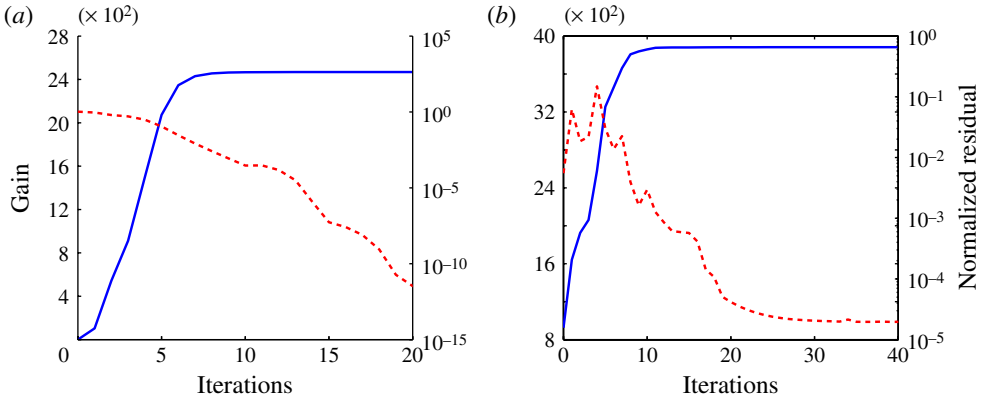

FIGURE 12. (Colour online) Gain $E(T)/E_0$ (blue solid line) and R_n (as defined in (2.17) and plotted with a red dashed line) plotted against iteration for (*a*) the $\mathrm{QLOP}_{T_{opt}}$ with $E_0 = 2.5 \times 10^{-8}$ (and $T = 182.5$), and (*b*) the $\mathrm{NLOP}_T^{(1)}$ perturbation with $E_0 = 3.2 \times 10^{-7}$ (and $T_{opt} = 205$).

branch have significantly enhanced gain occurring over a slightly longer optimization time than the perturbations on the QLOP_{T_Q} solution branch. Nevertheless, for all $\mathrm{NLOP}_{T_{opt}}^{(1)}$, the flow never undergoes a transition to turbulence, and so we believe this solution branch is completely distinct from the $\mathrm{NLOP}_{T_{opt}}^{(f)}$ solution branch, which approaches a minimal seed for turbulence as $E_0 \to E_c^-$.

Both these optimal perturbations exhibit good convergence properties as shown in figure 12, where (similarly to figures 4 and 9) we plot the gain and the normalized residual R_n against iteration for the $\mathrm{QLOP}_{T_{opt}}$ with $E_0 = 2.5 \times 10^{-8}$ (marked with a filled blue circle in figure 10) and the $\mathrm{NLOP}_{T_{opt}}^{(1)}$ with $E_0 = 3.2 \times 10^{-7}$ (marked with a filled magenta triangle in figure 10).

For the M11 flow geometry, the cross-over initial energy E_1 at which the $\mathrm{NLOP}_{T_{opt}}^{(1)}$ solution branch emerges with a larger gain than the $\mathrm{QLOP}_{T_{opt}}$ solution branch appears to be approximately $E_1 \simeq 7.5 \times 10^{-8}$. Interestingly, for initial energies $E_0 \simeq 1 \times 10^{-7}$, we are able using our algorithm to find either the QLOP_{T_Q} solution branch (the optimal time interval T_Q for this solution branch now being different from the globally optimal time interval T_{opt} for all initial conditions) or the $\mathrm{NLOP}_{T_{opt}}^{(1)}$ solution branch, depending on the particular form of the initial 'guess' for the perturbation. Even for energies larger than E_c, if we choose as an initial guess either random noise or the $\mathrm{NLOP}_{T_{opt}}^{(1)}$ near E_c, the algorithm converges to the $\mathrm{NLOP}_{T_{opt}}^{(1)}$ at that E_0 even for $E_c < E_0 \lesssim 2E_c$. This robust survival of the $\mathrm{NLOP}_T^{(1)}$ solution branch above E_c is thus analogous to the behaviour of the QLOP_T solution branch in the BF92 geometry, as discussed above.

Similar to the approach of M11, we estimate E_c by rescaling a turbulent seed found at large E_0 down in energy until the 'critical' T_c turbulent seed is found. This perturbation approaches very closely to the edge for an extended time period until eventually diverging and undergoing the transition to turbulence. (Although not reported in detail here, we conducted an edge-tracking procedure for the M11 geometry similar to that shown in figure 8 for the BF92 geometry, and thus were able

to identify the structure of the edge whose minimum energy state could be identified as the minimal seed for turbulence in this flow geometry.)

All of these observations are completely consistent with the schematic evolution shown in figure 2(*b*). For energies close to E_c, the emergence of the $\mathrm{NLOP}_T^{(f)}$ solution branch which converges to the minimal seed as $E_0 \to E_c$ is 'masked' not by the QLOP_{T_Q} solution branch, but rather by a distinct, inherently nonlinear solution branch which we refer to as the $\mathrm{NLOP}_{T_{opt}}^{(1)}$ solution branch, plotted in figure 2(*b*) with a thick grey line. This new solution branch appears in this flow geometry because the increased width and higher Re of this flow geometry allows localized perturbations of this form to undergo an initial (relatively brief) period of growth larger than that of the QLOP_{T_Q} with the same initial energy E_0, before 'unpacking' into a periodic, delocalized structure very similar in form to the QLOP_{T_Q}. This initial delocalization also explains why the optimal time T_{opt} for an $\mathrm{NLOP}_{T_{opt}}^{(1)}$ is somewhat longer than for a QLOP_{T_Q} (T_Q being typically very close to the optimal time for the underlying linear problem $T_L = 182.5$), as can be seen in figure 10.

Figures 13 and 14 allow us to compare the time evolution of $\mathrm{NLOP}_{T_{opt}}^{(1)}$ at $E_0 = 3.2 \times 10^{-7}$ to the time evolution of the identified minimal seed and the critical T_c turbulent seed. The contours of streamwise velocity u shown in figure 13 and the isosurfaces of u shown in figure 14 establish clearly that $\mathrm{NLOP}_{T_{opt}}^{(1)}$ converges to a structure very similar to the $\mathrm{QLOP}_{T_{opt}}$ shown in figure 11, with the conventional spanwise-periodic and streamwise-aligned streaks extending across the entire extent of the flow. Figure 14 also shows how the initially localized $\mathrm{NLOP}_{T_{opt}}^{(1)}$ unpacks into a series of streamwise streaks. An examination of the early time suggests that it is a combination of the Orr, oblique and lift-up mechanisms (as discussed in PWK12) that is responsible for the localized flow unpacking into streamwise streaks. These observations suggest that while at early time there exists a distinct localized perturbation associated with the inherently nonlinear $\mathrm{NLOP}_{T_{opt}}^{(1)}$ solution branch, which is able to extract enhanced gain from the base flow by 'unpacking', this solution branch at later times effectively matches onto the QLOP_{T_Q} solution branch to exploit the same lift-up mechanisms.

Turning now to a consideration of the time evolution of the minimal seed and the critical T_c turbulent seed (figures 13 and 14), it is clear that these perturbations also unpack in the streamwise and cross-stream directions, producing streamwise streaks which are still cross-stream localized. If there is just sufficient energy in these streaks, they are unstable, and the transition to turbulence occurs, as is the case for the turbulent seed. Otherwise the streaks persist, as is the case for the edge state reached from the minimal seed.

It is significant that the minimal and turbulent seeds are spanwise-localized (at least until the turbulence is reached) in this 2π wide geometry and not in the 1.05π wide geometry of BF92. Of course, the higher Re must be a contributory factor, but the spanwise dimension does seem important. PK10 originally found an azimuthally-localized (and radially-localized) inherently nonlinear optimal perturbation in a short pipe where one could talk about a 'spanwise' (azimuthal) length scale of 2π (radii or half-channel heights). The emergence of an inherently nonlinear and distinct solution branch (which we label as the $\mathrm{NLOP}_{T_{opt}}^{(1)}$ solution branch, as represented schematically in figure 2*b*) in the wider M11 geometry is also noteworthy. The linear optimal perturbation and, by definition, the associated quasi-linear optimal perturbation

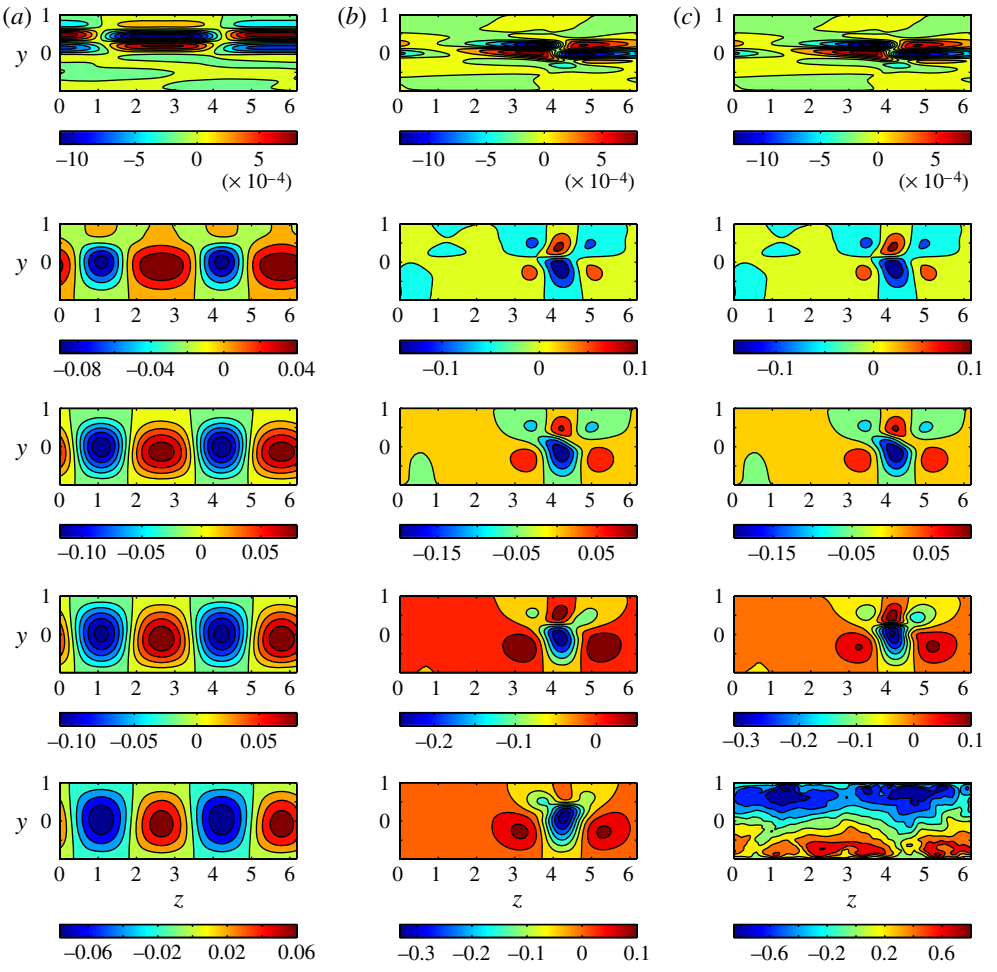

FIGURE 13. Contours of streamwise velocity u at times 0, 75, 150, 250 and 400 for the $\mathrm{NLOP}^{(1)}_{Topt}$ with $E_0 = 3.2 \times 10^{-7}$ marked in figure 10 with a filled magenta triangle (a, eventually decaying in amplitude), the edge state calculated by using the conventional bisection approach with $E_0 \simeq E_c$ (b) and the 'critical' T_c turbulent seed (c) for $E_0 = 3.25 \times 10^{-7} \gtrsim E_c$. Contour levels are: going down (a) (min, spacing, max) $= (-10, 2, 8) \times 10^{-4}$, $(-0.08, 0.02, 0.04)$, $(-0.1, 0.02, 0.08)$, $(-0.1, 0.02, 0.08)$, and $(-0.06, 0.02, 0.06)$; going down (b) (min, spacing, max) $= (-10, 2, 8) \times 10^{-4}$, $(-0.1, 0.05, 0.1)$, $(-0.15, 0.05, 0.1)$, $(-0.2, 0.05, 0.05)$ and $(-0.3, 0.05, 0.1)$; going down (c) (min, spacing, max) $= (-10, 2, 8) \times 10^{-4}$, $(-0.1, 0.05, 0.1)$, $(-0.15, 0.05, 0.1)$, $(-0.3, 0.05, 0.1)$ and $(-0.8, 0.2, 0.8)$.

are global periodic states which are largely insensitive to the geometry, whereas the gathering evidence is that it is possible within a nonlinear variational framework for inherently nonlinear optimal perturbations to arise as an attempt by the fluid to localize to maximize the energy gain for given global kinetic energy.

As is demonstrated here in the M11 geometry, it is entirely possible for nonlinear optimal perturbations, completely distinct in structure from the linear optimal perturbations to arise for ranges of initial energy $E_1 < E_0 < E_c$, and indeed for the minimal seed to be completely unrelated to both this solution branch and the quasi-linear optimal perturbation solution branch. It appears that the general trend should be

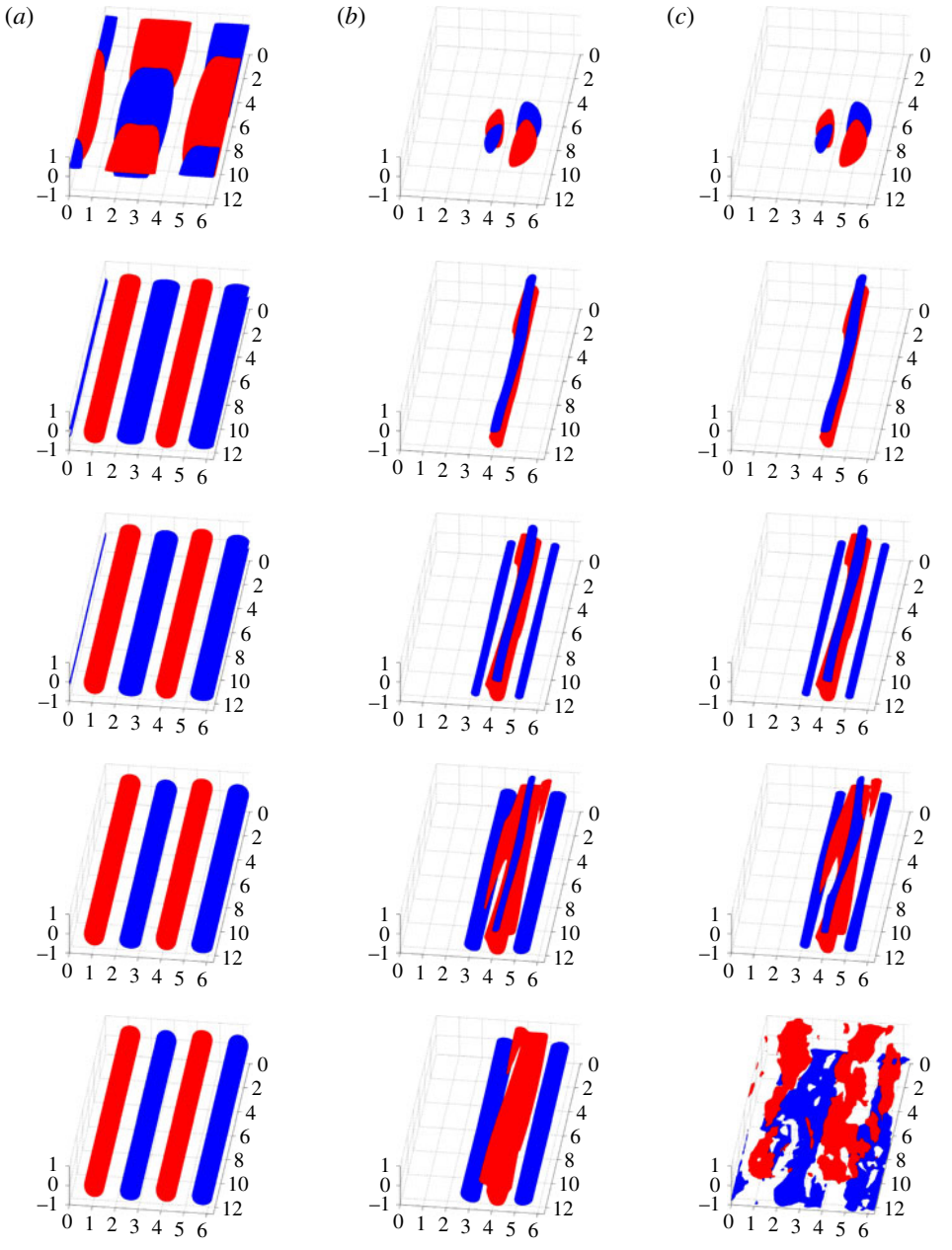

FIGURE 14. (Colour online) Isosurfaces of streamwise velocity u, at 60 % of maximum and minimum value, at times 0, 75, 150, 250 and 400, for (*a*) the $\mathrm{NLOP}^{(1)}_{T_{opt}}$ at $E_0 = 3.2 \times 10^{-7}$, (*b*) the edge state calculated by using the conventional bisection approach with $E_0 \simeq E_c$, and (*c*) the T_c turbulent seed at $E_0 = 3.25 \times 10^{-7}$.

that the energy cross-over (E_1) from quasi-linear optimal perturbations to inherently nonlinear optimal perturbations should decrease with increasing domain size. Clearly this cross-over is above E_c for the BF92 geometry at $Re = 1000$ and below E_c for the M11 geometry at $Re = 1500$.

Finally, it is interesting to note that the time-evolving structure of the critical turbulent seed, shown in figure 14(*c*), is at least qualitatively very reminiscent of the perturbation shown in figure 4 of M11 (albeit at a slightly different initial energy), suggesting that we have generated an approximation to the same (presumably unique) minimal seed. This is further supported by the aforementioned correspondence in their and our estimates for E_c. Beyond validating each other's results (which is important for nonlinear optimization problems), this points to an insensitivity in the choice of the functional to be maximized for finding the minimal seed. There is one proviso, of course, that the functional must be selected so that it detects turbulent flows by assuming large values. Only then will the variational procedure seek out turbulent seeds from amongst all the possible initial conditions with the same energy.

5. Conclusions

In this paper, we have sought the disturbance to plane Couette flow of a given finite kinetic energy E_0 which will experience the largest subsequent energy gain $G = E(T)/E_0$ where the time of maximum gain T is an *output* of our variational formulation. Two flow situations have been considered: $(L_x \times L_y \times L_z,\ Re) = (4.08\pi \times 2 \times 1.05\pi,\ 1000)$, as used for the original calculations of linear optimal perturbations in BF92, and $(4\pi \times 2 \times 2\pi,\ 1500)$, for which analogous nonlinear calculations have recently been performed optimizing the total dissipation over a specified period in M11. We have been particularly focused on assembling evidence to test the conjectures recently proposed by PWK12.

In both flow geometries, we have found an initial energy E_{fail} beyond which our variational algorithm no longer converges due to the existence of turbulence-triggering initial conditions, or 'turbulent seeds'. Therefore $E_{fail} \geqslant E_c$, the energy above which turbulence can be triggered. PWK12's first conjecture is that $E_{fail} = E_c$ if the energy hypersurface is sufficiently sampled, and we find nothing to contradict this conjecture. Indeed, by considering in detail the behaviour near to E_{fail} in the BF92 flow geometry, we find evidence that as E_0 approaches E_{fail} from below for a sufficiently long (and fixed) optimization time interval T, the variational algorithm finds a 'final' nonlinear optimal perturbation solution branch, which we refer to as the $\mathrm{NLOP}_T^{(f)}$ solution branch. Furthermore, it appears that as $E_0 \to E_{fail}^-$ the $\mathrm{NLOP}_T^{(f)}$ solution branch converges to a 'minimal seed', the state of minimum energy on the laminar–turbulent boundary, such that arbitrarily small perturbations of it lead to turbulence. This evidence gives further support to the first conjecture of PWK12, and also strongly supports their second conjecture, which proposes that the optimal perturbations for initial energies $E_0 = E_c - \epsilon^2$ for sufficiently small ϵ and sufficiently long optimization intervals will converge to the minimal seed as $\epsilon \to 0$.

Interestingly, in PCF, unlike the pipe flow considered by PWK12, this 'final' $\mathrm{NLOP}_T^{(f)}$ solution branch appears only for initial energies very close to E_c and large fixed T. If T is part of the optimization procedure, this solution branch $\mathrm{NLOP}_T^{(f)}$ is 'masked' by other perturbations, which attain larger maximum gain but over shorter time intervals. In the BF92 situation, for example, the quasi-linear optimal perturbation, $\mathrm{QLOP}_{T_{opt}}$, always has the largest maximum gain for $E_0 < E_c$, as illustrated schematically in figure 2 for $E_0 \lesssim E_c$. In M11, however, due to the wider flow geometry and higher Re, there also exists an intermediate range of initial energies $E_1 < E_0 < E_c$ in which the globally optimal (across all time intervals) initial perturbation is spatially localized, and so inherently nonlinear in character. This $\mathrm{NLOP}_{T_{opt}}^{(1)}$ solution branch has initially enhanced growth as it spatially 'unpacks' to

fill the entire flow geometry, but then subsequently behaves in a manner very similar to the $\mathrm{QLOP}_{T_{opt}}$. Also, in the M11 flow geometry, the failure of the convergence of our variational algorithm (which attempts to optimize energy gain at a specific target time) appears to give the same estimate for E_c and the same spatial structure of minimal seed as does an algorithm which optimizes the total dissipation over a long fixed time interval (as recently reported by M11). This confirms the 'robustness of failure' of the variational approach discussed by PWK12, in the sense that the estimation of E_c (or apparently equivalently E_{fail}) is insensitive to the exact optimization functional selected, provided that the functional assumes large values for turbulent flows (this condition is obviously key to ensuring that the variational procedure seeks out any 'turbulent seeds' if they exist at that energy level). Taken together, the evidence we have presented in this paper supports the belief that such a variational approach offers a fairly robust new theoretical tool to examine the nonlinear stability of fluid flows.

Many applications suggest themselves, but here we note just one: assessing the stabilizing or destabilizing influence of applied flow perturbations or controls. Normally, this would be attempted either by investigating the linearized operator around the base (laminar) flow or by carrying out exhaustive numerical simulations. The current work suggests a third way where the movement (in phase space) of the laminar–turbulent boundary towards (destabilization) or away (stabilization) from the base flow is investigated. We hope soon to report on some calculations along these lines.

6. Glossary

E_0	Initial energy of a perturbation for the optimization procedure.
E_{fail}	The minimum energy for which the optimization routine fails to converge.
E_c	The minimum energy of the edge (corresponding to the minimal seed) or equivalently the critical threshold energy to trigger turbulence.
T	The preset target time for the optimization procedure.
T_{opt}	The optimal time which emerges from the optimization procedure for maximum gain.
LOP_T	The linear optimal perturbation which is an initial condition giving rise to the largest gain after time T in the limit $E_0 \to 0$.
QLOP_T	The quasi-linear optimal perturbation is the finite-amplitude extension of LOP_T.
$\mathrm{QLOP}_{T_{opt}}$	QLOP_T where T is part of the optimization procedure.
NLOP_T	A fully nonlinear optimal perturbation which bears no relation to QLOP_T.
$\mathrm{NLOP}_{T_{opt}}$	NLOP_T where T is part of the optimization procedure.
$\mathrm{NLOP}_T^{(1)}$	The first NLOP_T found as E_0 increases from 0.
$\mathrm{NLOP}_{T_{opt}}^{(f)}$	The final NLOP_T found as E_0 increases towards E_c.
T_L	The time over which the gain is maximized in the linear problem.
T_Q	The time for which gain is maximized for the quasi-linear optimal perturbation.

Acknowledgements

We would like to thank A. Monokrousos and D. Henningson for helping us make contact with their work (M11), and the very insightful and constructive comments of three anonymous referees. S.M.E.R. would like to thank J. R. Taylor for his assistance with the installation and use of the Diablo CFD solver, S. B. Dalziel and A. Holyoake for their invaluable help with other computational issues and

G. Chandler for some insightful comments. S.M.E.R. is supported by a doctoral training award from EPSRC, and would like to acknowledge the Entente Cordiale Scholarship Scheme for support during the production of this manuscript. This work was performed using the Darwin Supercomputer of the University of Cambridge High Performance Computing Service (http://www.hpc.cam.ac.uk/), provided by Dell Inc. using Strategic Research Infrastructure Funding from the Higher Education Funding Council for England. The research activity of C.P.C. is supported by EPSRC Research Grant EP/H050310/1 'AIM (Advanced Instability Methods) for industry'. C.P.C. would also like to acknowledge the generous hospitality of the Hydrodynamics Laboratory (LadHyX) École Polytechnique/CNRS during the production of this manuscript.

REFERENCES

BOTTIN, S. & CHATE, H. 1998 Statistical analysis of the transition to turbulence in plane Couette flow. *Eur. Phys. J.* B **6** (1), 143–155.

BUTLER, K. M. & FARRELL, B. F. 1992 Three-dimensional optimal perturbations in viscous shear flow. *Phys. Fluids* A **4** (8), 1637–1650.

CHERUBINI, S., DE PALMA, P., ROBINET, J. C. & BOTTARO, A. 2010 Rapid path to transition via nonlinear localized optimal perturbations in a boundary-layer flow. *Phys. Rev.* E **82**, 066302.

CHERUBINI, S., DE PALMA, P., ROBINET, J. C. & BOTTARO, A. 2011*a* Edge states in a boundary layer. *Phys. Fluids* **23**, 051705.

CHERUBINI, S., DE PALMA, P., ROBINET, J. C. & BOTTARO, A. 2011*b* The minimal seed of turbulent transition in the boundary layer. *J. Fluid Mech.* **689**, 221–253.

DUGUET, Y., BRANDT, L. & LARSSON, B. R. J. 2010 Towards minimal perturbations in transitional Couette flow. *Phys. Rev.* E **82**, 026316.

DUGUET, Y., WILLIS, A. P. & KERSWELL, R. R. 2008 Transition in pipe flow: the saddle structure on the boundary of turbulence. *J. Fluid Mech.* **613**, 255–274.

GUSTAVSSON, L. H. 1991 Energy growth of three-dimensional disturbances in plane Poiseuille flow. *J. Fluid Mech.* **224**, 241–260.

ITANO, T. & TOH, S. 2001 The dynamics of bursting process in wall turbulence. *J. Phys. Soc. Japan* **70**, 703–716.

MONOKROUSOS, A., BOTTARO, A., BRANDT, L., DI VITA, A. & HENNINGSON, D. S. 2011 Nonequilibrium thermodynamics and the optimal path to turbulence in shear flows. *Phys. Rev. Lett.* **106** (13), 134502.

PRINGLE, C. C. T. & KERSWELL, R. R. 2010 Using nonlinear transient growth to construct the minimal seed for shear flow turbulence. *Phys. Rev. Lett.* **105** (15), 154502.

PRINGLE, C. C. T., WILLIS, A. P. & KERSWELL, R. R. 2012 Minimal seeds for shear flow turbulence: using nonlinear transient growth to touch the edge of chaos. *J. Fluid Mech.* **703**, 415–443.

REDDY, S. C. & HENNINGSON, D. S. 1993 Energy growth in viscous channel flows. *J. Fluid Mech.* **252**, 209–238.

REDDY, S. C., SCHMID, P. J., BAGGETT, J. S. & HENNINGSON, D. S. 1998 On the stability of streamwise streaks and transition thresholds in plane channel flows. *J. Fluid Mech.* **365**, 269–303.

ROMANOV, V. A. 1973 Stability of plane-parallel Couette flow. *Funct. Anal. Appl.* **7**, 137–146.

SCHMID, P. J. 2007 Nonmodel stability theory. *Annu. Rev. Fluid Mech.* **39**, 129–162.

SCHNEIDER, T. M., ECKHARDT, B. & YORKE, J. A. 2007 Turbulence transition and the edge of chaos in pipe flow. *Phys. Rev. Lett.* **99**, 034502.

SCHNEIDER, T. M., GIBSON, J. F., LAGHA, M., DE LILLO, F. & ECKHARDT, B. 2008 Laminar–turbulent boundary in plane Couette flow. *Phys. Rev.* E **78**, 037301.

SKUFCA, J. D., YORKE, J. A. & ECKHARDT, B. 2006 Edge of chaos in a parallel shear flow. *Phys. Rev. Lett.* **96**, 174101.

TAYLOR, J. R. 2008 Numerical simulations of the stratified oceanic bottom boundary layer. PhD thesis, University of California, San Diego.